August 2022

Ph.D. Dissertation

Cell selectivity, antimicrobial mechanism and anti-inflammatory activity of proadrenomedullin N-terminal 20 peptide and hybrid antimicrobial peptide

Graduate School of Chosun University

Department of Biomedical Sciences

Chelladurai Ajish

Cell selectivity, antimicrobial mechanism and anti-inflammatory activity of proadrenomedullin N-terminal 20 peptide and hybrid antimicrobial peptide

프로아드레노메둘린 아미노말단 20 펩타이드 및 하이브리드 항균 펩타이드의 세포선택성, 항균 작용기전 및 항염증 활성

2022년 8월 26일

Graduate School of Chosun University

Department of Biomedical Sciences

Cell selectivity, antimicrobial mechanism and anti-inflammatory activity of proadrenomedullin N-terminal 20 peptide and hybrid antimicrobial peptide

Advisor: Prof. Song Yub Shin

This dissertation is submitted to the Graduate School of Chosun University in partial fulfillment of the requirements for the degree of Doctor of Philosophy in Science

April 2022

Graduate School of Chosun University

Department of Biomedical Sciences

Chelladurai Ajish

Ph. D. Dissertation of

Chelladurai Ajish is certified by

Chairman (Chosun Univ.) : **Prof. Seung Joo Cho** .....

Committee Members:

Chosun Univ. : **Prof. Sung Tae Yang** .....

Chonnam Univ. : **Prof. Chul Won Lee** .....

Chosun Univ. : **Prof. Jung-Hee Lee** .....

Chosun Univ. : **Prof. Song Yub Shin** .....

June 2022

Graduate School of Chosun University

CONTENTS

LIST OF TABLES

PART I

PART II

LIST OF FIGURES

PART I

PART II

초 록

프로아드레노메둘린 아미노 말단 20 펩타이드 및 하이브리드 항균 펩타이드의 세포선택성, 항균작용 기전 및 항염증 활성

첼라두라이 아지쉬

지도교수: 신송엽, Ph.D.

의과학과

조선대학교 대학원

PART I

프로아드레노메둘린 N-말단 20 펩티드(PAMP)는 다양한 세포 유형에서 발견되는 조절 펩타이드이다. 그것은 많은 생물학적 활동에 관여하고 항균성 펩타이드(AMP)의 일반적인 특징인 염기성 및 소수성 아미노산이 풍부하다. 본 연구에서는 PAMP와 PAMP의 C-말단 펩타이드인 PAMP(9-20)의 세포선택성과 항균기전을 조사하였다. PAMP와 PAMP(9-20)는 표준 박테리아 균주에 대해 강력한 항균 활성(최소 억제 농도: 4-32 μM)을 나타내었지만 최고 측정농도인 256

μM에서도 용혈 활성을 나타내지 않았다. PAMP(9-20)는 PAMP에 비해 그람 음성균에 대한 항균 활성이 2~4배 증가하는 것으로 나타났다. 세포질 막 탈분극, 막 모방 리포솜에서 칼세인 염료 누출, SYTOX Green 흡수, 막 투과화 및 유세포 분석 연구는 PAMP 및 PAMP(9-20)의 주요 표적이 미생물 세포막이 아님을 나타냈다. 흥미롭게도, 레이저 스캐닝 공초점 현미경은 FITC로 표지된 PAMP와 PAMP(9-20)가 buforin-2와 유사한 대장균의 세포질에 들어가는 것을 보여주었고, 젤 지연 분석은 PAMP와 PAMP(9-20)가 박테리아 DNA에 효과적으로 결합한다는 것을 보여주었다. 이러한 결과는 세포내 표적 기전이 PAMP와 PAMP(9-20)의 항균작용을 담당함을 시사하였다. 종합하면, PAMP와 PAMP(9-20)는 새로운 항균제의 개발을 위한 유망한 후보물질로 간주될 수 있다.

PART II

2개의 알려진 항균 펩타이드(AMP)를 혼성화하는 것은 박테리아 세포에 대해 향상된 세포 선택성을 갖는 항균제를 설계하기 위한 간단하고 효과적인 전략이다. 본 연구에서 LfcinB6과 KR-12-a4가 Pro-

hinge와 연결된 하이브리드 펩타이드인 Lf-KR을 얻었다. 하이브리드 펩타이드 Lf-KR는 강력한 항균, 항염증 및 항생물막 활성을 가졌다. Lf-KR은 양 적혈구(sheep red blood cells)보다 세균 세포(bacterial cells)에 대해 우수한 세포 선택성(cell selectivity)을 나타내었다. Lf-KR은 시험된 12개의 박테리아 균주에 대해 광범위한 항균 활성(MIC: 4–8 μM)을 보여주었고, 생리학적 농도의 염(salt)이 존재할 때 항균 활성을 유지했다. 멤브레인 탈분극 및 염료 누출 분석은 Lf-KR의 향상된 항균 활성이 미생물 멤브레인의 투과 및 탈분극 증가로 인한 것임을 보여주었다. Lf-KR은 LPS로 자극된 마우스 대식세포 RAW264.7 세포에서 전염증성 사이토카인(산화질소 및 종양 괴사 인자-α)의 발현과 생성을 유의하게 억제하였다. 또한 Lf-KR은 미리 형성된 다제내성 녹농균(MDRPA) 생물막에 강력한 박멸 효과를 나타내었다. 아울러 미리 형성된 MDRPA 생물막 구조의 많은 부분이 Lf-KR의 첨가에 의해 교란되었음을 공초점 레이저 주사 현미경을 사용하여 확인했다. 종합적으로, 본 연구의 결과는 Lf-KR이 항균, 항염증 및 항생물막 약제로서 후보가 될 수 있음을 시사하였다.

ABSTRACT

Cell selectivity, antimicrobial mechanism and anti-inflammatory activity of proadrenomedullin N-terminal 20 peptide and hybrid antimicrobial peptide

Chelladurai Ajish
Advisor: Prof. Song Yub Shin
Department of Biomedical sciences
Graduate School of Chosun University

PART I

Proadrenomedullin N-terminal 20 peptide (PAMP) is a regulatory peptide that is found in various cell types. It is involved in many biological activities and is rich in basic and hydrophobic amino acids, a common feature of antimicrobial peptides (AMPs). In this study, the cell selectivity and antimicrobial mechanism of PAMP and its C-terminal peptide, PAMP (9-20), were investigated. PAMP and PAMP (9-20) displayed potent antimicrobial activity (minimum inhibitory concentration: 4-32 μM) against standard bacterial strains, but showed no hemolytic activity even at the highest tested concentration of 256 μM. PAMP (9-20) showed 2- to 4-fold increase in antimicrobial activity against gram-negative bacteria compared to PAMP. Cytoplasmic membrane depolarization, leakage of calcein dye from membrane mimic liposomes, SYTOX Green uptake, membrane permeabilization, and flow cytometry studies indicated that the major target of PAMP and PAMP (9-20) is not the microbial cell membrane. Interestingly, laser-scanning confocal microscopy demonstrated that FITC-labeled PAMP

and PAMP (9-20) enter the cytoplasm of *Escherichia coli* similar to buforin-2, and gel retardation assay indicated that PAMP and PAMP (9-20) effectively bind to bacterial DNA. These results suggest that the intracellular target mechanism is responsible for the antimicrobial action of PAMP and PAMP (9-20). Collectively, PAMP and PAMP (9-20) could be considered promising candidates for the development of new antimicrobial agents.

PART II

Hybridizing two known antimicrobial peptides (AMPs) is a simple and effective strategy for designing antimicrobial agents with enhanced cell selectivity against bacterial cells. Here, we generated a hybrid peptide Lf-KR in which LfcinB6 and KR-12-a4 were linked with a Pro hinge to obtain a novel AMP with potent antimicrobial, anti-inflammatory, and anti-biofilm activities. Lf-KR exerted superior cell selectivity for bacterial cells over sheep red blood cells. Lf-KR showed broad-spectrum antimicrobial activities (MIC: 4–8 μM) against tested 12 bacterial strains and retained its antimicrobial activity in the presence of salts at physiological concentrations. Membrane depolarization and dye leakage assays showed that the enhanced antimicrobial activity of Lf-KR was due to increased permeabilization and depolarization of microbial membranes. Lf-KR significantly inhibited the expression and production of pro-inflammatory cytokines (nitric oxide and tumor necrosis factor-α) in LPS-stimulated mouse macrophage RAW264.7 cells. In addition, Lf-KR showed a powerful eradication effect on preformed multidrug-resistant *Pseudomonas aeruginosa* (MDRPA) biofilms. We confirmed using confocal laser scanning microscopy that a large portion of the preformed MDRPA biofilm structure was perturbed by the addition of Lf-

KR. Collectively, our results suggest that Lf-KR can be an antimicrobial, anti-inflammatory, and anti-biofilm candidate as a pharmaceutical agent.

PART I

Proadrenomedullin N-terminal 20 peptide (PAMP) and its C-terminal 12-residue peptide, PAMP (9-20): Cell selectivity and antimicrobial mechanism

1. Introduction

Proadrenomedullin N-terminal 20 peptide (PAMP) is a biologically active molecule (20 amino acid residues) produced by post-translational enzymatic processing of the common precursor of adrenomedullin (AM), a 185-amino acid proadrenomedullin molecule [1]. Although AM and PAMP both have hypotensive effects in the cardiovascular system, they also exert diverse and distinct effects on endocrine physiology, innate immunity, cytoskeletal biology, and receptor signaling pathways [2]. Similar to AM, PAMP is potently expressed and secreted by adrenal chromaffin cells but is also widely found throughout the body, including the plasma and urine [3]. Kuwasako et al. identified the C-terminal 12-residues of PAMP [PAMP (9-20)] in porcine adrenal medulla as a major endogenous active peptide of the AM precursor and demonstrated that its hypotensive activity is comparable to that of PAMP [4]. The physicochemical property of PAMP is similar to that of many antimicrobial peptides (AMP). For example, it has a net positive charge of +4 at neutral pH owing to an excess of basic amino acids (Arg and Lys). Further, it is rich in hydrophobic residues such as Trp, Leu, Val, and Phe. Marutsuka et al. [5] demonstrated that PAMP can significantly inhibit Escherichia coli growth in a dose-dependent manner. Its antimicrobial activity was comparable or superior to that of other known AMPs such as human β-defensin-2 (hBD-2) and neutrophil peptide-1 (HNP-1) [5].

Aside from their relatively cheaper manufacturing cost, short AMPs are commonly preferred for therapeutic applications due to their lower toxicity. Thus, shorter analogs of PAMP are desired. The presence of anionic Asp4 and Glu8 residues in the N-terminal region of PAMP may prevent the electrostatic interaction of the peptide with the negatively charged phospholipids of bacterial outer membrane. PAMP (9-20) is more basic and amphipathic than PAMP. Hence, in this study, to address whether PAMP (9-20) possess antimicrobial activity, its antimicrobial activity against gram-positive and gram-negative standard bacterial strains was tested and compared with PAMP. We also examined their hemolytic activity against sheep red blood cells. To further gain

insight into the mechanism of their antimicrobial action, we performed cytoplasmic membrane depolarization, leakage of calcein dye from bacterial membrane mimic liposomes, SYTOX Green uptake, membrane permeabilization, flow cytometry, laser-scanning confocal microscopy, and DNA gel retardation assays.

2. Materials and Methods

2.1 Materials

Calcein, 3-(4,5-dimethylthiazol-2-yl)-2,5-diphenyl-2H-tetrazolium bromide (MTT), N-phenyl-1-napthylamine (NPN), egg yolk L-phosphatidylethanolamine (EYPE), egg yolk L-phosphatidyl-DL-glycerol (EYPG) were purchased from Sigma-Aldrich (St. Louis, MO, USA). SYTOX Green was obtained from Life Technologies (Eugene, OR, USA). 3,3′-Dipropylthiadicarbocyanine iodide (diSC3-5) was supplied from Molecular Probes (Eugene, OR, USA).

2.2 Peptide synthesis

PAMP and PAMP (9-20) are synthesized by solid-phase synthesis using Fmoc (N-(9-fluorenylmethoxy carbonyl) chemistry. The peptides were purified by reversed-phase preparative HPLC on a C18 column (250mm × 20mm; Vydac) using an appropriate 0-90% H2O/CH3CN gradient in the presence of 0.05% trifluoroacetic acid. The purity (≥ 95%) and hydrophobicity were analyzed by reversed-phase analytical HPLC on C18 column (4.6 mm × 250 mm; Vydac) (Fig. S1). The molecular masses of purified peptides were determined by ESI-MS (electrospray ionization-mass spectrometry) (Framingham, MA, USA) (Fig. S2). FITC-labeled PAMP and PAMP (9-20) synthesized by coupling FITC to amine group of linker 6-aminocaproic acid were purchased from ANYGEN (Gwangju, Korea).

2.3Antimicrobial assay

Bacterial strains were including gram-negative and gram-positive bacteria were supplied from the Korean Collection for Type Cultures (KCTC) (Daejeon, Korea). The minimal inhibitory concentration (MIC) of the peptides was determined according to a previously described method [6]. In brief, bacterial cells were grown to mid mid-log phase and diluted in 0.1% peptone to a final concentration of 4 × 106 CFU/ml. Subsequently, the peptides were serially diluted in 0.1% peptone and then mixed with equal volumes of bacterial solution in a 96-well microtiter plates. After incubation for 18–24 h at 37 °C, the lowest concentration

of peptide that prevented visible turbidity was defined as the MIC.

2.4 Hemolytic activity assay

Fresh sheep red bloods were washed with PBS and 4% blood solution was prepared in PBS. In a 96-well plate, 100 µl of varying concentrations of peptides were prepared. Another 100 µl of 4% blood solution was added to each well. The plate as then incubated for 1 h at 37°C. The plate was centrifuged and the OD450 of the supernatant was measured. 1% triton-X100 was taken a positive control and PBS was taken as a negative control.

2.5 Cytoplasmic membrane depolarization assay

The cytoplasmic membrane depolarization activity of the peptides was determined with the membrane potential-sensitive fluorescent dye, diSC3-5, as previously described [7]. Briefly, logarithmic growing S. aureus (KCTC 1621) cells were harvested and diluted to OD600 = 0.05 in 5 mM HEPES buffer (pH 7.4, containing 20 mM glucose). The cell suspension was further incubated with 0.4 µM diSC3-5 and 100 mM K+ until no further reduction of fluorescence. The fluorescence was recorded (excitation λ = 622 nm, emission λ = 670 nm) with a Shimadzu RF-5300PC fluorescence spectrophotometer (Kyoto, Japan). Subsequently, 3 ml of cell suspension was added to a 1 cm quartz cuvette and mixed with the peptides at their 2×MIC. Changes in the fluorescence were recorded from 0 to 500 s.

2.6 SYTOX Green uptake assay

To quantify membrane permeabilization of S. aureus (KCTC 1621) caused by the peptides the SYTOX green assay as previously described [8]. Briefly, logarithmic growing S. aureus (KCTC 1621) suspensions of 2 × 106 CFU/ml in buffer (20 mM glucose, 5 mM HEPES and 10 mM KCl, pH 7.4) were prepared and mixed with 1 mM SYTOX Green at 37 ℃ for 15 min in the dark. After the addition of the peptides to the final concentration corresponding to 2 × MIC, the uptake of SYTOX Green was determined using a Shimadzu RF-5300PC fluorescence spectrophotometer (Kyoto, Japan) with an excitation wavelength of 485 nm and

an emission wavelength of 520 nm.

2.7 Dye leakage assay

Prepared calcein-entrapped large unilamellar vesicles (LUVs) were optimized using a previous method [9]. The negatively charged lipids composed of EYPE/EYPG (7:3, w/w) were dissolved in chloroform, dried with a stream of nitrogen and resuspended in dye buffer solution (70 mM calcein, 10 mM Tris, 150 mM NaCl, and 0.1 mM EDTA, pH 7.4). The suspension was subjected to 10 freeze-thaw cycles in liquid nitrogen and extruded 21 times through a LiposoFast-Extruder (Avestin, Inc., Canada) equipped with filters of 100 nm pore size. Untrapped calcein was removed from the liposome by gel filtration on a Sephadex G-50 column Calcein leakage from liposomes was monitored at room temperature by measuring fluorescence intensity at an excitation wavelength of 490 nm and emission wavelength of 520 nm on a Shimadzu RF-5300PC fluorescence spectrophotometer (Kyoto, Japan). Complete dye release was obtained using 0.1 % Triton X-100.

2.8 Outer membrane (OM) permeabilization assay

The outer membrane-permeabilizing activity of the peptide was determined by using the fluorescent dye NPN (1-N-phenylnaphthylamine) assay as previously described [10]. Briefly, logarithmic growing E. coli (KCTC 1682) were collected and diluted to OD600 = 0.2 in 5 mM HEPES buffer (pH 7.4) containing 5 mM glucose. The cell suspension was further incubated with 10 μM NPN. Subsequently, the different concentrations of the peptides were added to 3 ml of cell suspension in a 1 cm quartz cuvette. The fluorescence was detected (excitation λ = 350 nm, emission λ = 420 nm) with a Shimadzu RF-5300PC fluorescence spectrophotometer (Kyoto, Japan).

2.9 Inner membrane (IM) permeabilization assay

The inner membrane permeabilizing ability of the peptides was determined by measurement of cytoplasmic β-galactosidase activity in E. coli ML-35 cells with ONPG (o-nitrophenyl-β-D-galactoside) as the substrate, as described previously [11]. Briefly, E. coli ML-35 cells were washed thrice in 10 mM PBS (pH 7.4)

containing 1.5 mM ONPG and were diluted to an OD600 of 0.05. Then, 150 µl of bacterial culture was added to 50 µl of PBS containing the peptide at different concentrations in each well of sterile 96-well plates. The rate of inner membrane permeability was assessed by the hydrolysis of ONPG to o-nitrophenol determined by reading the absorbance at 405 nm. The hydrolysis of ONPG to o-nitrophenol, taken as an indicator of the permeability status of the inner membrane, was monitored by measuring the OD at 405 nm.

2.10 Flow cytometric analysis

Integrity of bacterial cell membrane was assessed by measuring the propidium iodide (PI) uptake by flow cytometry, as described previously [12]. Briefly, mid-log phase S. aureus cells were diluted to until the OD600 absorbance was approximately 0.4. Then, the bacteria suspension was further diluted 10 times with 10 mM PBS (pH 7.4). Peptide at 2 × MIC was added, and the mixture was incubated for 30 min at 37 °C. Then add PI with final concentration of 10µg/ml and incubate for 30 min. Finally, PI fluorescence was collected by a FACScan instrument (FACSCalibur, Beckman Coulter Inc., USA)

2.11 Confocal laser-scanning microscopy

E. coli (KCTC 1682) cells were cultured in LB broth to mid log phase and harvested by centrifugation. The cell pellets were washed three times with PBS. Bacteria (106 CFU/mL) cells were incubated with FITC-labeled peptides (30 µM) for 20 min at 37 °C. After incubation, the cells were harvested by centrifugation and then washed three times using PBS (pH 7.4) and fixed on a glass slide. The images of cells with FITC-labeled samples were collected using a Leica TCS SP5 confocal laserscanning microscope (Leica Microsystems, Germany)

2.12 DNA binding assay

To examine peptide binding to DNA, an agarose gel-retardation assay was performed as previously described [13]. Briefly, peptide samples were mixed with a fixed concentration (100 ng) of plasmid DNA (pBR322) in a sample buffer (10 mM Tris-HCl, 5% glucose, 50 µg/mL BSA, 1 mM EDTA, and 20 mM KCl). The mixture of DNA and peptide was incubated at 37 °C for 1 h. After incubation, the

samples were analyzed by 1% agarose gel electrophoresis in 0.5% TAE buffer. The plasmid bands were detected by UV illuminator (Bio-Rad, USA).

3. Results

3.1. Synthesis and physicochemical properties of the peptides

The sequence, molecular mass, net charge, ratio of hydrophobic amino acids, hydrophobic moment, and HPLC retention time (Rt) of PAMP and PAMP (9-20) are listed in Table 1. Their net charge and hydrophobic moment were calculated using the HeliQuest analysis website (http://heliquest.ipmc.cnrs.fr/cgi-bin/ComputParamsV2.py). The analytical RP-HPLC retention time of PAMP was 20.884 min, while PAMP (9-20), which lacks the N-terminal 8-residues of PAMP, had a reduced retention time of 15.426 min, indicating a decrease in hydrophobicity. The α-helical-wheel diagram for PAMP and PAMP (9-20) are shown in Fig. 1. As shown in Table 1, PAMP (9-20) was more basic and amphipathic than PAMP.

3.2 Antimicrobial and hemolytic activities

PAMP and PAMP (9-20) displayed the same antimicrobial activity against gram-positive bacteria (Table 2). In contrast, PAMP (9-20) showed a 2- or 4-fold increased antimicrobial activity against gram-negative bacteria compared to PAMP (Table 2). To determine their potential cytotoxic effect on mammalian cells, the hemolysis induced by the peptides in sheep red blood cells (sRBCs) was examined. Even at the highest tested concentrations of 256 μM, they had no hemolytic activity (Fig. S3).

3.3 Cell selectivity (therapeutic index)

The therapeutic potential of AMPs is assessed by their cell selectivity to eradicate bacterial cells as opposed to normal mammalian cells. The cell selectivity of the peptides was calculated using the formula, therapeutic index (TI) = HC10/GM, where HC10 is the peptide concentration that induces 10% lysis of sRBCs and GM is the geometric mean of minimum inhibitory concentrations (MICs) against all tested bacteria (Table 3). The estimated TI is an important index indicating the balance between drug effect and toxicity. A higher TI value represented better cell selectivity as well as therapeutic potential. Compared to a natural AMP (melittin),

PAMP and PAMP (9-20) showed increased TI values of 24.9- and 39.4-fold, respectively (Table 3). These results suggested that PAMP and PAMP (9-20) possess an optimized structure that produce much greater cell selectivity against bacterial cells over mammalian cells. Additionally, PAMP (9-20) displayed a 1.6-fold increased TI value than PAMP.

3.4 Cytoplasmic membrane depolarization

Upon the permeabilization and disruption of the outer and inner membrane, the electrical potential changes of the cytoplasmic membrane (CM) were measured by the membrane potential-sensitive dye, diSC3-5. Under normal conditions, this cationic dye is concentrated in the cytoplasmic membrane, leading to self-quenching of the fluorescence. However, once the CM was disturbed due to perturbation of the ion flux, diSC3-5 was taken up into the cytoplasm where it formed a monomer with the continued production of fluorescence. As shown in Fig. 2A, the depolarization by 2 × MIC of the peptides was monitored over a period of 500 seconds. Melittin, well known as membrane-disrupting AMP, induced rapid and complete membrane depolarization for Staphylococcus aureus within 50 seconds. However, PAMP and PAMP (9-20) did not cause any membrane depolarization at 2 × MIC similar to buforin-2, which is well known as an intracellular targeting AMP.

3.5 SYTOX Green uptake assay

The SYTOX Green uptake assay was conducted to further examine the effect of PAMP and PAMP (9-20) on membranes (Fig. 2B). SYTOX Green is a membrane-impermeable nucleic acid stain that only enters membrane-disrupted cells. The influx of SYTOX Green by membrane permeabilization of S. aureus was recorded after exposure to the peptides. A rapid and complete increase in SYTOX green influx was seen at 2 × MIC (8 μM) of melittin within 50 seconds. However, similar to buforin-2, no SYTOX green influx was observed at 2 × MIC (32 μM) of PAMP and PAMP (9-20).

3.6 Calcein dye leakage

Dye leakage assay is usually conducted to evaluate whether PAMP and PAMP (9-20) exert antimicrobial activity by pore formation and/or membrane perturbation (Fig. 2C). Egg yolk phosphatidyl-ethanolamine (EYPE) and Egg yolk phosphatidyl-glycerol (EYPG) were used to mimic the negatively charged cytoplasmic membrane of bacteria. We measured the ability of PAMP (9-20) to induce calcein leakage from negatively charged EYPE/EYPG (7:3, w/w) LUVs. As expected, melittin caused a rapid and high level of calcein leakage in negatively charged LUVs, indicating that liposomes were destroyed by pore formation. However, like buforin-2, PAMP and PAMP (9-20) did not induce any dye leakage at 4 μM.

3.7 Outer membrane permeabilization

The ability of PAMP and PAMP (9-20) to permeabilize the outer membrane (OM) of E. coli was determined by NPN uptake assay (Fig. 2D). Normally, NPN is a hydrophobic fluorescent probe that is quenched in aqueous environments but strongly fluoresces in hydrophobic environments. Under normal conditions, the OM of a bacterial cell is impermeable to NPN. However, permeabilization of the OM allows NPN to enter the hydrophobic environment of the membrane, thereby leading to enhanced fluorescence in the cell. Hence, the increased fluorescence of NPN indicated a weakening or loss of the OM structure of bacteria. As shown in Fig. 2D, melittin was able to permeabilize the outer membrane of E. coli in a dose-dependent manner. Like buforin-2, PAMP and PAMP (9-20) induced relatively low permeabilization of the outer membrane of E. coli.

3.8 Inner membrane permeabilization

To further investigate the inner membrane permeabilization of PAMP and PAMP (9-20), ortho-nitrophenyl-β-galactoside (ONPG) assay was conducted using the membrane defective bacterium E. coli ML-35 (Fig. 2E). Usually, E. coli ML-35 cannot transfer extracellular ONPG into the cytoplasm due to the lack of lactose permease. With the induced permeabilization of the inner membrane, ONPG could enter the cytoplasm and be decomposed into o-nitrophenol through β-

galactosidase, which generates absorbance at 420 nm. Melittin induced inner membrane permeability in a dose-dependent manner. Similar to buforin-2, PAMP and PAMP (9-20) did not induce inner membrane permeabilization even at 64 μM.

3.9 FACScan analysis

We tested whether PAMP and PAMP (9-20) could permeabilize the membrane integrity of E. coli by propidium iodide (PI) uptake assay (Fig. 3). PI is a fluorescent dye that does not penetrate the integral bacterial membrane. Nevertheless, when the membrane is damaged, PI dye enters the bacteria staining nucleic acids and binds to bacterial DNA, resulting in fluorescence increase. To quantitatively determine the degree to which the bacterial membrane was damaged, flow cytometric analysis by PI uptake was carried for E. coli treated with the peptides. Fig. 6 demonstrated that the control (without peptide) produced only 1.50 % PI positive bacterial cells, indicating viable cell membranes. In the presence of melittin at 2 × MIC, PI was taken up, and a strong PI fluorescence of 90.12% was seen, respectively. In contrast, like buforin-2, PAMP and PAMP (9-20) did not cause any alteration in membrane permeability at 2 × MIC (< 5% of PI positive cells).

3.10 Confocal laser-scanning microscopy

To determine the site of action of PAMP and PAMP (9-20), FITC-labeled PAMP and FITC-labeled PAMP and PAMP (9-20) were incubated with log phase E. coli and their localization was visualized by confocal laser-scanning microscopy. E. coli cells treated for half an hour with FITC-labeled buforin-2, PAMP, and PAMP (9-20) at room temperature appeared as green rods with fluorescence spread throughout the bacterial cell, indicating internalization of FITC-labeled peptide into the cytoplasm of the bacteria (Fig. 4A).

3.11 DNA binding activity

To explore intracellular targeting mechanism, we compared the DNA binding affinity of PAMP and PAMP (9-20). The gel retardation assay was conducted by

analyzing the electrophoretic mobility of DNA bands at various concentrations of the peptides to DNA on an agarose gel (1%, w/v). As shown in Fig. 4B, buforin-2, PAMP, and PAMP (9-20) started retardation at a concentration of 2, 4, and 4 μg/mL, respectively. Buforin-2 and PAMP (9-20) completely inhibited DNA migration through the gel at 8 and 4 μg/mL, respectively.

4. Discussion

In addition to PAMP, it was found that PAMP (9-20) acts as an antimicrobial peptide. PAMP (9-20) exhibits more potent antimicrobial activity against gram-negative bacteria compared to PAMP. Despite their potent antimicrobial activity (MIC: 4-32 μM), PAMP and PAMP (9-20) were not hemolytic and cytotoxic even at 256 μM and 128 μM, respectively. Hence, PAMP and PAMP (9-20) overcame the main limiting factors of natural AMPs (melittin) and have the potential to be developed into therapeutic agents. According to previous studies, most AMPs exert antimicrobial activities by damaging cytoplasmic membrane integrity [14,15]. In addition to the membrane-target mechanism, it is known that some AMPs such as buforin-2 and indolicidin can lead to cellular inactivation by binding to intracellular targets (e.g., DNA, RNA or proteins) [13,16,17]. Using various fluorophore-based studies including cytoplasmic membrane depolarization, SYTOX Green uptake, NPN uptake, ONPG hydrolysis, and flow cytometry, we investigated the effect of PAMP and PAMP (9-20) on bacterial membrane and demonstrated that PAMP (9-20) did not affect the integrity of bacterial membrane. To exclude the possibility that nonlipid components influence the activity of PAMP and PAMP (9-20) on the membrane and further confirm that PAMP and PAMP (9-20) have the ability to affect the microbial plasma membrane, we investigated their effect on the integrity of artificial liposome LUVs, which were composed of EYPE and EYPG (7:3, w/w), as a model for the bacterial plasma membrane. The results showed that PAMP and PAMP (9-20) did not disrupt the integrity of these negatively charged LUVs, implying that PAMP (9-20) is inactive against both—bacterial plasma membrane as well as the bacterial membrane model. Importantly, laser-scanning confocal microscopy revealed the translocation of PAMP and PAMP (9-20) to the interior of the bacterial cells, and gel retardation assay showed that they directly bound to bacterial DNA as an intracellular target. Particularly, the DNA binding ability of PAMP (9-20) was much stronger than that of PAMP. Overall, considering the data obtained in this study, the antimicrobial action of PAMP and PAMP (9-20)

seem to exert via an intracellular target. However, Martinez et al. reported that the free-acid (-OH form) and mature form (-NH2 form) of PAMP are very efficient in increasing outer membrane permeability in a manner similar to polymyxin B, suggesting that the mechanism underlying the antimicrobial activity of PAMP involves punching holes in the bacterial outer membrane [18].

5. Conclusion

In the present study, we have demonstrated that short peptide PAMP (9-20) has comparable, or superior antimicrobial activity to PAMP. Various fluorophore-based studies revealed that the major target of PAMP and PAMP (9-20) is not the bacterial membrane. Laser-scanning confocal microscopy and gel retardation assay demonstrated that intracellular target mechanisms are responsible for the antimicrobial actions of PAMP and PAMP (9-20). Collectively, PAMP and PAMP (9-20) could be considered promising molecules for the development of new antimicrobial agents.

Table 1. Amino acid sequence and physicochemical properties of PAMP and PAMP(9-20).

Peptides	Amino acid sequence	Net charge	H[a]	μH[b]	t_R (min)[c]	Average Mass (Da)	MS Analysis[d] z	m/z calc.	m/z found
							2	1231.9	1231.9
		4	45	0.272	20.884	2461.8	3	821.6	821.6
PAMP	ARLDVASEFRKKWNKWALSR-NH_2						4	616.5	616.3
							1	1620.9	1620.1
		5	41.7	0.399	15.426	1619.9	2	810.9	810.2
PAMP(9-20)	FRKKWNKWALSR-NH_2						3	540.9	541

[a] hydrophobic amino acid ratio (%)
[b] Hydrophobicity moment (μH) were calculated online at: http://heliquest.ipmc.cnrs.fr/cgi-bin/ComputParams.py.
[c] Retention times (t_R) were determined by analytical RP-HPLC on a C_{18} column (5 mm; 4.6 mm × 250 mm; Vydac) using a gradient of buffer B (0.05% TFA in CH_3CN/H_2O 90:10 v/v) in buffer A (0.05 %TFA in H_2O) for 60 min with a flow rate of 1.0 mL/min.
[d] Molecular masses were determined by electrospray ionization-mass spectrometry (ESI-MS). Z: ion charge, m/z: mass to charge ratio

Table 2. Antimicrobial activity of PAMP and PAMAP(9-20) against gram-negative and gram-positive bacterial standard strains.

	Minimal Inhibitory Concentration (MIC)[a] (mM)					
	Gram-negative bacteria			Gram-positive bacteria		
Peptides	*E. coli* [KCTC 1682]	*P. aeruginosa* [KCTC 1637]	*S. typhimurium* [KCTC 1926]	*B. subtilis* [KCTC 3068]	*S. epidermidis* [KCTC 1917]	*S. aureus* [KCTC1621]
PAMP	8	32	16	8	8	16
PAMP(9-20)	4	16	4	8	8	16
melittin	2	4	4	4	4	4

a MIC (minimum inhibitory concentration) was determined as the lowest concentration of peptide that caused 100 % inhibition of microbial growth.

Table 3. GM, HC_{10} and therapeutic index (TI) of the peptides

Peptides	GM (μM)[a]	HC_{10} (μM)[b]	TI[c]	Fold
PAMP	14.7	> 256	34.8	24.9
PAMP (9-20)	9.3	> 256	55.1	39.4
melittin	3.7	5	1.4	1.0

[a] The geometric mean (GM) of the MIC was obtained from Table 2.
[b] HC10 is the minimum peptide concentration that caused >10 % hemolysis of sheep red blood cells.
[c] Therapeutic index (TI) is the ratio of the HC_{10} value (μM) over GM (μM). When no detectable hemolytic activity was observed at 256 μM, a value of 512 μM was used to calculate the therapeutic index (TI). Larger values indicate greater cell selectivity.

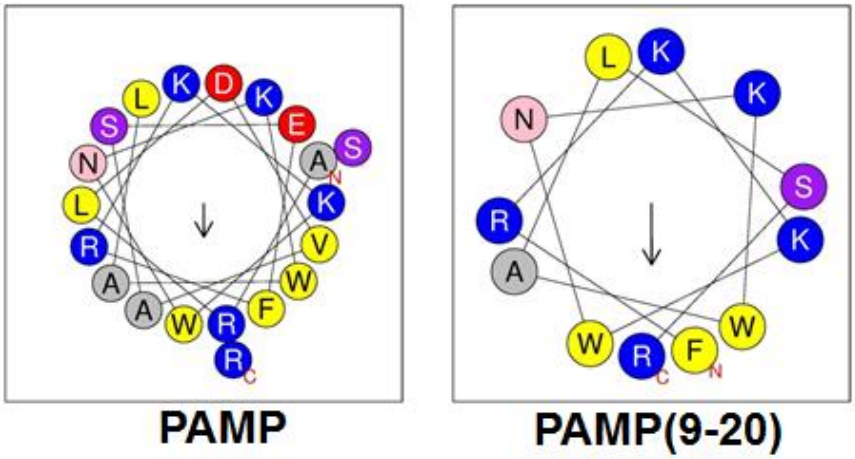

Figure. 1. The a-helical wheel plots of PAMP and PAMP (9-20) are drawn using the HeliQuest tool (http://heliquest.ipmc.cnrs.fr/). Positively charged residues (polar) and hydrophobic (nonpolar) residues are represented as blue circles and yellow circles, respectively. (For interpretation of the references to colour in this figure legend, the reader is referred to the Web version of this article.)

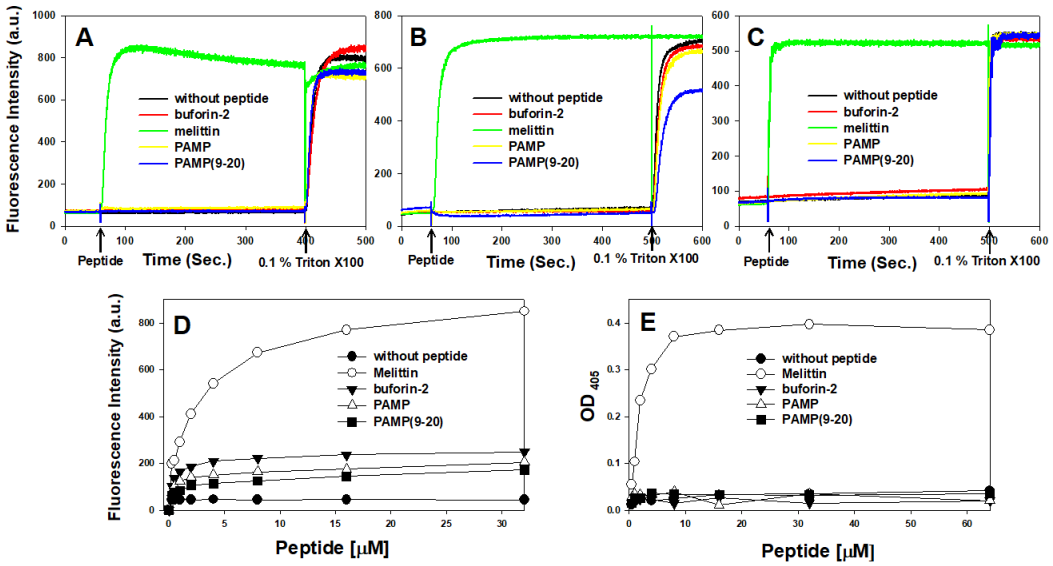

Figure. **2**. (A) Cytoplasmic membrane depolarization of Staphylococcus aureus (KCTC 1621) treated with the peptides (2 × MIC). (B) SYTOX green uptake of S. aureus (KCTC 1621) treated with the peptides (2 × MIC). (C) Calcein leakage induced by the peptides against large unilamellar vesicles (LUVs) composed of egg yolk phosphatidyl-ethanolamine (EYPE)/egg yolk phosphatidyl-glycerol (EYPG) (7:3, w/w). (D) Outer membrane permeability of the peptides. Membrane uptake of 1-N-phenylnaphthylamine (NPN) by E. coli (KCTC 1682) in the presence of different concentrations of the peptides. (E) Inner membrane permeability of the peptides. Hydrolysis of ortho-Nitrophenyl-b-galactoside (ONPG) due to release of cytoplasmic b-galactosidase in E. coli ML-35 cells treated with peptides. (For interpretation of the references to colour in this figure legend, the reader is referred to theWeb version of this article.)

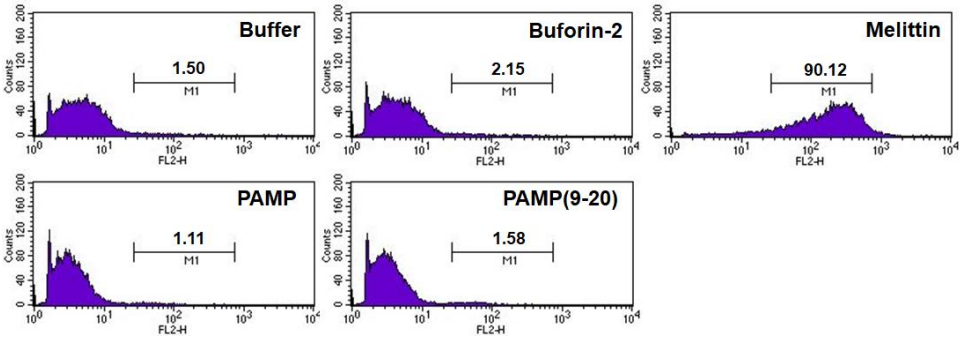

Figure. **3**. Cytoplasmic membrane integrity of S. aureus (KCTC 1621) treated with the peptides ((2 × MIC), as measured by an increase in fluorescent intensity of propidium iodide (10 mg/mL) at 4°C for 30 min. The control was processed without peptides..

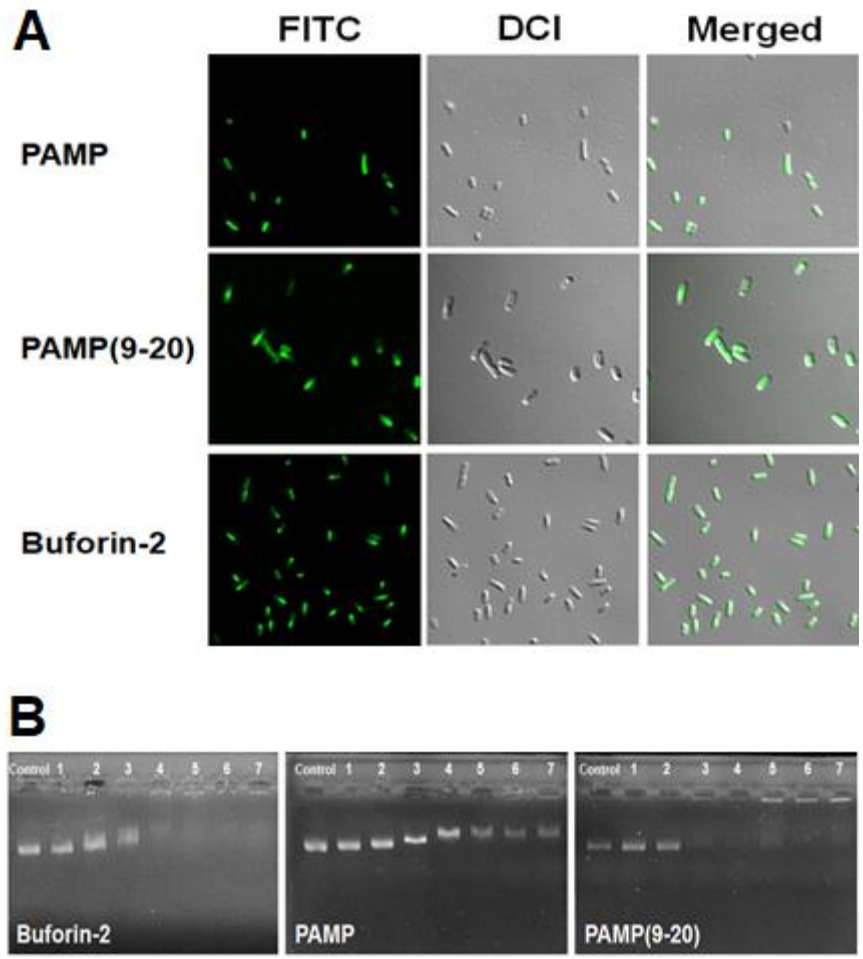

Figure. **4**. (A) Localization of fluorescein isothiocyanate (FITC) labeled peptides on bacteria. Approximately 106 CFU/mL of E. coli (KCTC 1682). The bacterial cells were incubated with FITC labeled peptides. Bacteria were washed and fixed, and images were acquired using confocal laser-scanning microscopy. (B) Gel retardation assay. Binding was assayed based on the inhibitory effect of peptides on the migration of DNA bands. Control, plasmid DNA; lane 1, 1 μM; lane 2, 2 μM; lane 3, 4 μM; lane 4, 8 μM; lane 5, 16 μM; lane 6, 32μM; and lane 7, 64 μM.

References

[1] K. Kitamura, J. Sakata, K. Kangawa, et al., Cloning and characterization of cDNA encoding a precursor for human adrenomedullin, Biochem. Biophys. Res. Commun. 194 (1993) 720–725.

[2] B.C. Matson, M. Li, C.E. Trincot, et al., Genetic loss of proadrenomedullin N-terminal 20 peptide (PAMP) in mice is compatible with survival, Peptides 112 (20) 96–100.

[3] H. Washimine, K. Kitamura, Y. Ichiki, et al., Immunoreactive proadrenomedullin N-terminal 20 peptide in human tissue, plasma and urine, Biochem. Biophys. Res. Commun. 202 (1994) 1081–1087.

[4] K. Kuwasako, K. Kitamura, Y. Ishiyama, et al., Purification and characterization of PAMP-12 (PAMP[9-20]) in porcine adrenal medulla as a major endogenous biologically active peptide. FEBS Lett. 414 (1997)105-110.

[5] K. Marutsuka, Y. Nawa, Y. Asada, et al., Adrenomedullin and proadrenomudullin N-terminal 20 peptide (PAMP) are present in human colonic epithelia and exert an antimicrobial effect, Exp. Physiol. 86 (2001) 543–545.

[6] J. Nam, H. Yun, G. Rajasekaran, et al., Structural and functional assessment of mBjAMP1, an antimicrobial peptide from Branchiostoma japonicum, revealed a novel α-Hairpinin-like scaffold with membrane permeable and DNA binding activity, J. Med. Chem. 61 (2018) 11101–11113.

[7] C.L. Friedrich, D. Moyles, T.J. Beveridge, et al., Antibacterial action of structurally diverse cationic peptides on gram-positive bacteria, Antimicrob. Agents Chemother. 44 (2000) 2086–2092.

[8] E.Y. Kim, G. Rajasekaran, S.Y. Shin, LL-37-derived short antimicrobial peptide KR-12-a5 and its d-amino acid substituted analogs with cell selectivity, anti-biofilm activity, synergistic effect with conventional antibiotics, and anti-inflammatory activity, Eur. J. Med. Chem. 136 (2017) 428–441.

[9] A.A. Stromstedt, M. Pasupuleti, A. Schmidtchen, et al., Evaluation of strategies for improving proteolytic resistance of antimicrobial peptides by using variants of EFK17, an internal segment of LL-37. Antimicrob. Agents Chemother. 53 (2009) 593–602.

[10] B. Jacob, Y. Kim, J.K. Hyun, et al., Bacterial killing mechanism of sheep myeloid antimicrobial peptide-18 (SMAP-18) and its Trp-substituted analog with improved cell selectivity and reduced mammalian cell toxicity, Amino Acids 46 (2014) 187–198.

[11] R. I. Lehrer, A. Barton, K. Daher, et al., Interaction of human defensins with *Escherichia coli.* mechanism of bactericidal activity, J. Clin. Invest. 84 (1989) 553−561.

[12] S. Joshi, G.S. Bisht, D.S. Rawat, et al., Interaction studies of novel cell selective antimicrobial peptides with model membranes and *E. coli* ATCC 11775, Biochim. Biophys. Acta 1798 (2010) 1864–1875.

[13] C.B. Park, H.S. Kim, S.C. Kim, Mechanism of action of the Antimicrobial peptide buforin II: buforin II kills microorganisms by penetrating the cell membrane and inhibiting cellular functions, Biochem. Biophys. Res. Commun. 244 (1998) 253–257.

[14] L. Xu, S. Chou, J. Wang, et al., Antimicrobial activity and membrane-active mechanism of tryptophan zipper-like β-hairpin antimicrobial peptides, Amino Acids 47 (2015) 2385-2397.

[15] J. Li, J.J. Koh, S. Liu, Membrane Active Antimicrobial Peptides: Translating Mechanistic Insights to Design. Front Neurosci. 11 (2017) 73.

[16] C.B. Park, K.S. Yi, K. Matsuzaki, et al., Structure-activity analysis of buforin II, a histone H2A-derived antimicrobial peptide: the proline hinge is responsible for the cell-penetrating ability of buforin II, Proc. Natl. Acad. Sci. U. S. A. 97 (2000) 8245–8250.

[17] C. Subbalakshmi, N. Sitaran, Mechanism of antimicrobial action of indolicin, FEMS Microbiol. Lett. 160 (1998) 91–96.

[18] A. Martinez, J.A. Bengoechea, F. Cuttitta, Molecular evolution of proadrenomedullin N-terminal 20 peptide (PAMP): evidence for gene cooption, Endocrinology 147 (2006) 3457–3461.

Supplementary data

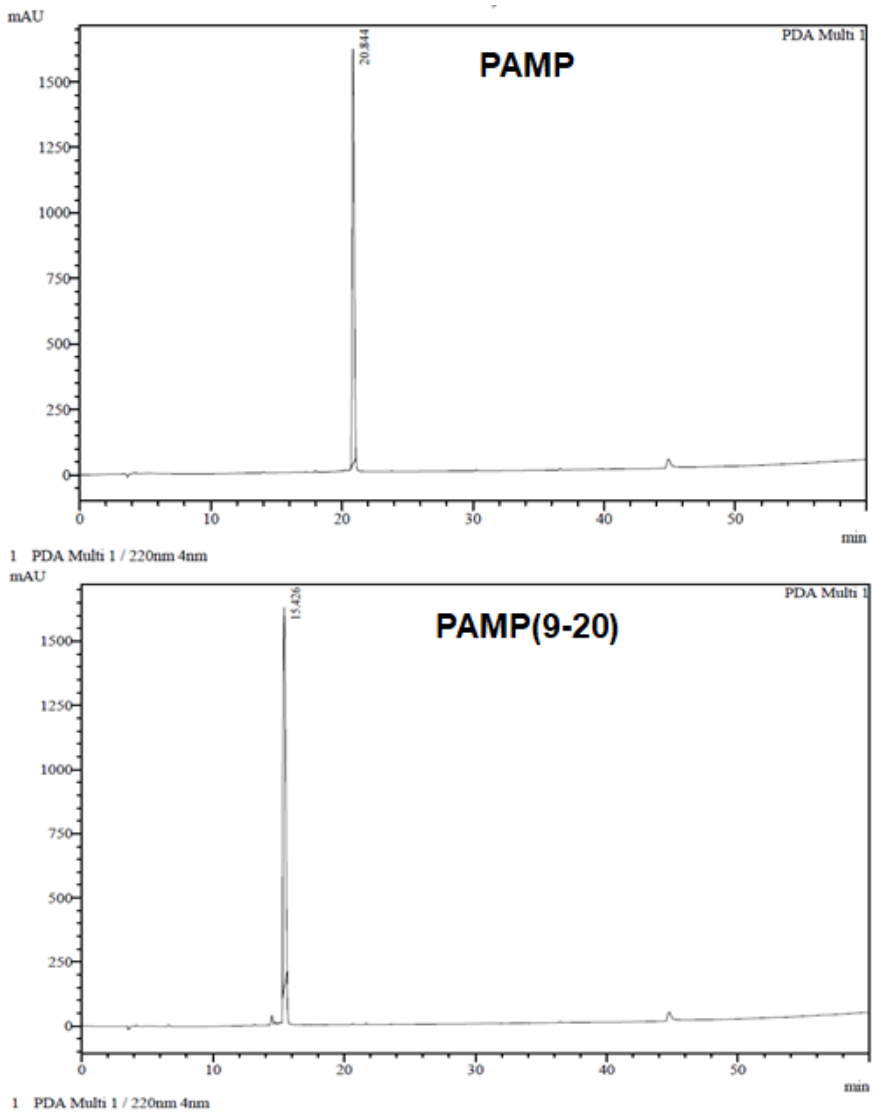

Fig. S1. Analytical RP-HPLC profiles of Synthetic PAMP and PAMP (9-20). Peptides were eluted for 60 min with a flow rate of 1.0 mL/min by analytical RP HPLC on a C_{18} column (5 mm; 4.6 mm × 250 mm; Vydac) using a gradient of buffer B (0.05% TFA in CH_3CN/H_2O 90:10 v/v) in buffer A (0.05 %TFA in H_2O).

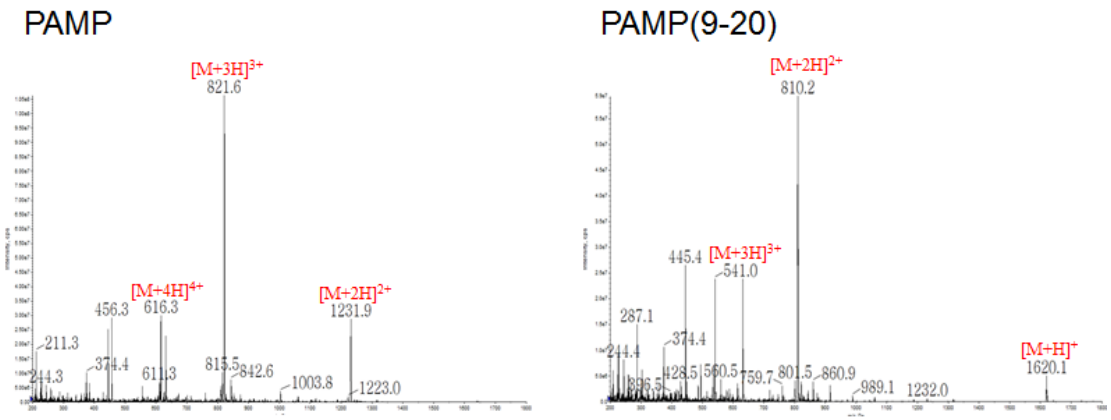

Peptides	Molecular MS								
	Calculated					Observed			
	Mw	$[M+H]^{1+}$	$[M+2H]^{2+}$	$[M+3H]^{3+}$	$[M+4H]^{4+}$	$[M+H]^{1+}$	$[M+2H]^{2+}$	$[M+3H]^{3+}$	$[M+4H]^{4+}$
PAMP	2461.8	2462.8	1231.9	821.6	616.5	-	1231.9	821.6	616.3
PAMP(9-20)	1619.9	1620.9	810.9	540.9	405.9	1620.1	810.2	541.0	-

Fig. S2. Electrospray ionization-mass spectrometry (ESI-MS) spectra of PAMP and PAMP (9-20)

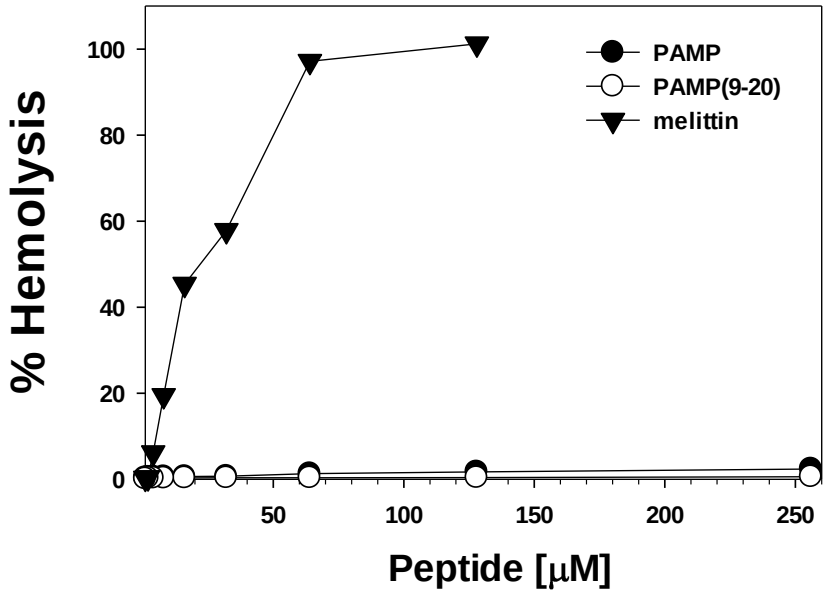

Fig. S3. Hemolytic activity of the peptides against sheep red blood cells

PART II

A novel hybrid peptide composed of LfcinB6 and KR-12-a4 with enhanced antimicrobial, anti-inflammatory and anti-biofilm activities

1. Introduction

The increasing emergence and dissemination of antibiotic resistance have become a global public health challenge[1]. Therefore, there is an urgent need to develop new antimicrobial agents to overcome this problem. In recent years, antimicrobial peptides (AMPs) have attracted considerable interest as promising therapeutic alternatives to conventional antibiotics because of their broad-spectrum antimicrobial activity, membrane-targeting antimicrobial mechanism, rapid killing, and infrequent development of drug resistance[2,3]. AMPs are an essential component of the innate immune system and are produced as the first line of defense by multicellular organisms[2,3]. Furthermore, they possess immunomodulatory properties such as leukocyte recruitment and suppression of harmful inflammation[3]. One strategy to design novel AMPs with enhanced antimicrobial activity while reducing cytotoxicity is to combine two AMPs into a hybrid peptide. Hybrid peptides preserve the original amino acid residues from natural AMPs, and some special additional sequences are chosen to enhance antimicrobial activity and reduce hemolytic activity compared to natural AMPs. Currently, hybrid AMPs have been developed by combining several amino acid residue sequences from different AMPs. One of the first hybrid AMP is the hybridization of cecropin A (CA) and melittin (ME). These CA-ME hybrids are more potent than either the parental CA or ME against bacterial strains including methicillin-resistant *Staphylococcus aureus* (MRSA) with reduced hemolysis[4,5]. Hybrid peptides, LfcinB-PG and CA-PG derived from three AMPs, protegrin-1 (PG), bovine lactoferricin (LfcinB) and CA exhibited enhanced cell selectivity and potent anti-inflammatory activity.[6] In addition, the hybrid peptides, LI, LN, and LC designed by combining the typical fragment of human cathelicidin LL-37 with either indolicidin, pig nematode cecropin P1 (CP-1) or rat neutrophil peptide-1 (NP-1) displayed higher antimicrobial activity and lower hemolytic activity than its parental peptides[7].

LfcinB is a 25-residue multi-functional cationic AMP produced by pepsin digestion from the N-terminal region of bovine lactoferrin (LF), an 80 kDa iron-binding glycoprotein[8]. LfcinB6 (RRWQWR-NH_2) is the antimicrobial core sequence of LfcinB[9]. It has been reported to be the smallest motif that exhibits antimicrobial activity[10]. KR-12 is the shortest antimicrobial sequence of the human cathelicidin AMP, LL-37[11]. As an analog of KR-12, KR-12-a4 (KRIVKLIKKWLR-NH_2) is known to exhibit potent antimicrobial activity against gram-positive and gram-negative bacteria and relatively high LPS-neutralization activity[12]. In this study, we designed a hybrid peptide, Lf-KR, composed of LfcinB6 and KR-12-a4, to generate a novel AMP with enhanced cell selectivity for bacterial cells and LPS-neutralization activity along with minimal cytotoxicity. Here, Pro kink was introduced between LfcinB6 and KR-12-a4 to provide cell selectivity. Pro kinks in several α-helical AMPs are known to provide cell selectivity[13-15]. Although Pro is commonly known as a helix-breaking amino acid, it has been found in the putative transmembrane helices of integral membrane proteins[16]. It has been proposed that Pro kink in the membrane-spanning helices facilitates gating by the channel[16]. Also, a number of α-helical membrane-active AMPs including melittin, caerin 1.1, buforin-2, gaegurins, and piscidins contain one or two Pro residues in their central portion[17-20]. One or two Pro residues in these AMPs disturbs the hydrogen bond patterns in the middle of the helix, leading to helix-hinge-helix structures. Introduction of Pro at the central position of some α-helical AMPs increased cell selectivity for bacterial cells than introduction of Gly or Ala[20-22]. For this reason, we chosen Pro as the linker in hybrid peptide Lf-KR.

The minimal inhibitory concentration (MIC) against gram-positive and gram-negative bacterial strains was determined to evaluate the antimicrobial activities (including antibiotic-resistant bacteria) of the peptides. Toxicity was assessed by determining hemolytic activity against sheep red blood cells. The effect of monovalent and/or multivalent ions on the antimicrobial activity of the peptides was also investigated. The secondary conformation of the peptides was

measured in different aqueous solutions and a membrane mimicking environment by circular dichroism (CD) spectroscopy.

In addition to their direct antimicrobial activity, some AMPs including human cathelicidin LL-37, bovine indolicidin, and defensin are known to suppress lipopolysaccharide (LPS)-induced inflammatory responses by neutralizing and binding LPS[23-26]. Here, the anti-inflammatory activity of the Lf-KR hybrid peptide was established by investigating nitric oxide (NO) and tumor necrosis factor (TNF)-α cytokine release and their mRNA expression in LPS-stimulated RAW cells.

Biofilms are multicellular aggregates of surface-associated microorganisms that are estimated to cause at least 65% of all infections in humans, particularly implantable device-related infections and chronic disease infections[27,28]. Biofilm-related infections are very difficult to treat in the clinic because of their adaptive resistance to most antibiotics and consequent recalcitrance to treatment with conventional antibiotics. Consequently, there is an urgent need for drugs that effectively treat biofilm-associated infections.

Therefore, we investigated the anti-biofilm activity against multidrug-resistant Pseudomonas aeruginosa (MDRPA) biofilms to evaluate the potential of Lf-KR as a new anti-biofilm agent. The potency of the hybrid peptide to eradicate preformed MDRPA biofilms was evaluated as the minimum biofilm eradication concentration (MBEC). Furthermore, the anti-biofilm activity of Lf-KR on mature MDRPA biofilms was investigated by quantitative analysis of biofilm morphology using a laser confocal scanning microscope (CLSM).

2. Materials and Methods

2.1 Materials

Egg yolk L-phosphatidylethanolamine (EYPE), egg yolk L-phosphatidyl-DLglycerol (EYPG), LPS purified from Escherichia coli O111:B4, were purchased from Sigma-Aldrich (St. Louis, MO, USA). 3,3′-Dipropylthiadicarbocyanine iodide ($diSC_3$-5), SYTO 9 and propidium iodide (PI) were supplied from Molecular Probes (Eugene, OR, USA). HyClone Dulbecco's modified Eagle's medium (DMEM) and fetal bovine serum (FBS) were obtained from SeouLin Bioscience (Seoul, Korea). The enzyme-linked immunosorbent assay (ELISA) kits for TNF-α were procured from R&D Systems (Minneapolis, MN).

2.2 Bacterial strains.

Bacterial strains were chosen to detect the minimal inhibitory concentration (MIC) of the peptides, as previously described[55]. Three strains of gram-positive bacteria (*Bacillus subtilis* [KCTC 3068], *Staphylococcus epidermidis* [KCTC 1917], and Staphylococcus aureus [KCTC 1621]) and three strains of gram-negative bacteria (*Escherichia coli* [KCTC 1682], *Pseudomonas aeruginosa* [KCTC 1637], and Salmonella typhimurium [KCTC 1926]) were procured from the Korean Collection for Type Cultures (KCTC) of the Korea Research Institute of Bioscience and Biotechnology (KRIBB). Methicillin-resistant *Staphylococcus aureus* (MRSA) [CCARM 3089, CCARM 3090, and CCARM 3095] and multidrug-resistant *Pseudomonas aeruginosa* strains (MDRPA) [CCARM 2095, and CCARM 2109] were obtained from the Culture Collection of Antibiotic-Resistant Microbes (CCARM) of Seoul Women's University in Korea. Vancomycin-resistant *Enterococcus faecium* (VREF) [ATCC 51559] was supplied from the American Type Culture Collection (Manassas, VA, USA).

2.3 Peptide synthesis and characterization.

Peptides are synthesized using solid-phase peptide synthesis employing a fluorenylmethoxycarbonyl (Fmoc) protecting group strategy[56]. The peptides were

purified by reversed-phase preparative HPLC on a C18 column (250 mm × 20 mm; Vydac) using an appropriate 0–90% H_2O/CH_3CN gradient in the presence of 0.05% trifluoroacetic acid. The purity (≥95%) and hydrophobicity were analyzed by reversed-phase analytical HPLC on C18 column (4.6 mm ×250 mm; Vydac). The molecular masses of purified peptides were determined by ESI-MS (electrospray ionization-mass spectrometry) (Framingham, MA, USA).

2.4 Bioinformatic analysis.

The α-helical wheel plot, net charge and hydrophobic moments were calculated online using the HeliQuest server. The three-dimensional structure of Hybrid-LK was predicted online using I-TASSER server[29].

2.5 Circular dichroism (CD) spectroscopy.

CD studies were done in a JACSO-(J-715) spectropolarimeter (Jasco, Japan) with 0.1 mm quartz cuvette at 25ºC. The peptides were dissolved in 10 mM sodium phosphate buffer (pH 7.4), 50% TFE, and 30 mM SDS micelles. The percentage of α-helix of the peptides was calculated using the following equation, α-helix (%) = $-100 \times (\theta_{222} + 3000)/33000$.

2.6 Minimum inhibitory concentration (MIC).

The minimal inhibitory concentrations (MICs) of the peptides against bacterial strains were determined via the broth microbroth dilution protocol recommended by the Clinical and Laboratory Standard Institute (CLSI)[30,34]. In brief, mid-logarithmic phase of bacteria was diluted with Mueller-Hinton broth (MHB) (Difco, USA) and added to a microtiter 96-well plate (2×10^6 CFU/well). A two-fold serial dilution of samples (concentration range: 1–64μM) was subsequently added, and the plate was incubated for 24 h at 37 ℃. The MIC (mg/L) was taken as the lowest concentration of the antimicrobial that inhibited the visible growth of the bacteria. All experiments were performed in triplicate and included growth and sterility controls.

2.7 Hemolytic activity.

The hemolytic activity of the peptides was determined as the amount of hemoglobin released by the lysis of sheep red blood cells (sRBCs), as previously described[55]. Briefly, fresh sheep red bloods were washed with PBS and 4% blood solution was prepared in PBS. In a 96-well plate, 100 µl of varying concentrations of peptides were prepared. Another 100 µl of 4% blood solution was added to each well. The plate as then incubated for 1 h at 37°C. The plate was centrifuged and the OD_{450} of the supernatant was measured. 0.1% triton-X100 was taken a positive control and PBS was taken as a negative control.

2.8 Cytoplasmic membrane depolarization assay.

The cytoplasmic membrane depolarization activity of the peptides was determined with the membrane potential-sensitive fluorescent dye, diSC_3-5, as previously described[43]. Briefly, logarithmic growing S. aureus (KCTC 1621) cells were harvested and diluted to OD_{600} = 0.05 in 5 mM HEPES buffer (pH 7.4, containing 20 mM glucose). The cell suspension was further incubated with 0.4 µM diSC_3-5 and 100 mM K^+ until no further reduction of fluorescence. The fluorescence was recorded (excitation λ = 622 nm, emission λ = 670 nm) with a Shimadzu RF-5300PC fluorescence spectrophotometer (Kyoto, Japan). Subsequently, 3 ml of cell suspension was added to a 1 cm quartz cuvette and mixed with the peptides at their 2×MIC. Changes in the fluorescence were recorded from 0 to 500 s.

2.9 Dye leakage assay.

Prepared calcein-entrapped large unilamellar vesicles (LUVs) were optimized using a previous method[57]. The negatively charged lipids composed of EYPE/EYPG (7:3, w/w) were dissolved in chloroform, dried with a stream of nitrogen and resuspended in dye buffer solution (70 mM calcein, 10 mM Tris, 150 mM NaCl, and 0.1 mM EDTA, pH 7.4). The suspension was subjected to 10 freeze-thaw cycles in liquid nitrogen and extruded 21 times through a LiposoFast-Extruder (Avestin, Inc., Canada) equipped with filters of 100 nm pore size. Untrapped calcein was removed from the liposome by gel filtration on a

Sephadex G-50 column Calcein leakage from liposomes was monitored at room temperature by measuring fluorescence intensity at an excitation wavelength of 490 nm and emission wavelength of 520 nm on a Shimadzu RF-5300PC fluorescence spectrophotometer (Kyoto, Japan). Complete dye release was obtained using 0.1 % Triton X-100.

2.10 Cytotoxicity against RAW264.7 macrophage cells.

The cytotoxicity of the peptides against mouse macrophage RAW264.7 cells was assessed by MTT assay[58]. Briefly, RAW264.7 cells were cultured in DMEM (Gibco) with 10% FBS in a humidified atmosphere containing 5% CO2 at 37 °C. The cells were added to 96-well plates at a final concentration for 2×10^4 cells per well in DMEM and cultured overnight. TZP4 was then added and incubated for 48 hr. MTT (50 µL, 0.5 mg/mL) was added to the 96-wellplate and incubated at 37 °C for 4 hr. Subsequently, 150 µL of DMSO was added to dissolve the formed formazan crystals after the supernatant was discarded, and the OD was measured using a microplate reader (Bio-Tek Instruments EL800, USA) at 550 nm. Cell viability was expressed as (A_{550nm} of treated sample) / (A_{550nm} of control) 100%.

2.11 Measurement of nitric oxide or tumor necrosis factor-α release from LPS-stimulated RAW264.7 cells.

Peptide-induced inhibition of nitric oxide (NO) and proinflammatory cytokine, tumor necrosis factor (TNF)-α production in LPS-stimulated macrophage cells were measured as previously described[59]. In brief, RAW264.7 murine macrophage cells (2 ×106 cell/mL) were plated and adhered to a 96 well plates (100 mL/well) and stimulated with LPS from *E. coli* O111:B4 (20 ng/mL) in the presence or absence of peptide for 24 h. After 24 h incubation, the culture supernatant was collected for enzyme linked immunosorbent assay (ELISA) to detect the level of nitric oxide (NO) and inflammatory cytokine TNF-α. The nitrite level was determined using Griess reagent (1% sulfanilamide, 0.1% naphthylethylenediamine dihydrochloride and 2% phosphoric acid). Release of

TNF-α was detected using DuoSet ELISA mouse TNF-α (R&D Systems, Minneapolis, USA) according to the manufacturer's protocol.

2.12 Reverse-transcription polymerase chain reaction (RT-PCR).

RT-PCR was performed as previously described[55]. RAW264.7 cells were plated into 6-well plates at a concentration of 5×10^5 cells/well and stimulated with *E. coli* O111:B4 LPS (20 ng/mL) in the presence or absence of the peptides. After incubation of 3 h (for TNF-α) and 6 h [for inducible nitric oxide synthase (iNOS)], total RNA was extracted using TRIzol® reagent (Invitrogen) and RNA concentration quantified using Nanodrop spectrophotometer (BioDrop, UK). cDNA was synthesized from 2 μg of total RNA using Oligo-d(T)15 primers and PrimeScript Reverse Transcriptase kit (Takara, Japan) according to the manufacturer's protocol. The cDNA products were amplified using following primers: iNOS (forward 5´-CTGCAGCACTTGGATCAGGAACCTG-3´, reverse 5´-GGGAGTAGCCTGTGTGCACCTGGAA-3´); TNF-α (forward 5´-CCTGTAGCCCACGTCGTAGC-3´, reverse 5´-TTGACCTCAGCGCTGAGTTG-3´) and GAPDH (forward 5´-GAGTCAACGGATTTGGTCGT-3´, reverse 5´-GACAAGCTTCCCGTTCTCAG-3´). The PCR amplification was carried out at initial denaturation at 94 ℃ for 5 min, followed by forty cycles of denaturation at 94 ℃ for 1 min, annealing at 55 ℃ for 120 sec and extension at 72 ℃ for 1 min, with a final extension at 72 ℃ for 5min. The PCR products were separated by electrophoresis and visualized under UV illumination.

2.13 LPS-binding assay.

The LPS-binding ability of the peptides was determined by a BODIPY-TRcadaverine (BC) displacement assay[60,61]. Briefly, LPS from *E. coli* O111:B4 (25 μg/ml) was incubated with BC (2.5 μg/ml) and peptide (1-32 μM) in Tris buffer (50 mM, pH 7.4) for 4 hr. A volume of 2ml of this mixture was added to a quartz cuvette. Fluorescence was recorded at an excitation wavelength of 580 nm and an emission wavelength of 620 nm with a Shimadzu RF-5301 PC fluorescence spectrophotometer (Shimadzu Scientific Instruments). The

percentage fluorescence was calculated using formula: $\%\Delta F\ (AU) = [(F_{obs} - F_0)/(F_{100} - F_0)] \times 100$, where F_{obs} is the observed fluorescence at a given peptide concentration, F_0 is the initial fluorescence of BC with LPS in the absence of peptides, and F_{100} is the BC fluorescence with LPS cells upon the addition of 10 μg/ml polymyxin B.

2.14 Biofilm eradication assay (MBEC).

Biofilm eradication, determined as the MBEC of the peptides, was assessed according to methods from the literature using the Calgary Biofilm Device (Innovotech, Edmonton, Canada)[62,63]. Briefly, 1×10^6 CFU/mL of bacteria were suspended in 150 μL of appropriate nutrient media (LB media) and placed in 96-well microtiter plates with peg lids (Innovotech, Edmonton, Canada; product code: 19111) to establish biofilms. Plates were sealed with parafilm and incubated at 37 °C for 24 h in a shaking incubator at 110 rpm. Lids of the plates were then removed, rinsed with 0.01 M PBS, and transferred to sterile 96-well plates containing serial dilutions of the peptides: the final volume with the media was 200 μL/well. Plates were then incubated at 37 °C for 24 h in a shaking incubator at 110 rpm. After 24 h of treatment, the peg lid of each plate was removed, rinsed with buffer, and transferred to a recovery plate containing 200 μL of nutrient media. Recovery plates were thereafter sonicated in a water bath for 10–15 min to dislodge biofilms. Peg lids were removed and plates were incubated overnight (for 24 h) at 37 °C in a shaking incubator at 110 rpm to recover viable bacteria, resulting in turbidity. The MBEC values were recorded as the lowest concentration resulting in eradication of the biofilm (i.e., no turbidity after the final incubation period relative to sterility controls). Experiments were performed in triplicates, and the median value of each experiment was presented.

2.15 Confocal laser scanning fluorescence microscopy (CLSM).

MDRPA (1×10^6 CFU/mL) was cultured in 24-well plates containing discs placed in MHB-glucose medium, for 24 h to form biofilms. Discs with planktonic cells were washed with 1× PBS thrice and placed in fresh 24-well plates containing Lf-KR (MBEC: 16 μM), and plates were incubated for 6 h. Discs were

removed, washed twice with 1 × PBS, and concomitantly stained with 6.7 μM SYTO 9 and 40 μM PI. After incubation in the dark at 37 °C for 30 min, planar images of biofilm mass in the discs were visualized using CLSM (Zeiss LSM 710 Meta, ZEISS Microscopy, Jena, Germany), and analyzed using ZEN 2009 Light Edition software (ZEISS Microscopy, Jena, Germany).

Rink amide-methylbenzhydrylamine (MBHA) resin, 9-fluorenyl-methoxycarbonyl (Fmoc) protected amino acids, and other chemicals and solvents used for peptide synthesis were bought from Novabiochem (La Jolla, CA, USA). LPS purified from *Escherichia coli* O111:B4, 2,2,2-trifluoroethanol (TFE), sodium dodecyl sulfate (SDS), 3-(4,5-dimethylthiazol-2-yl)-2,5-diphenyl-2H-tetrazolium bromide (MTT), ciprofloxacin, oxacillin and chloramphenicol, were supplied from Sigma-Aldrich (St. Louis, MO, USA). HyClone Dulbecco's modified Eagle's medium (DMEM) and fetal bovine serum (FBS) were obtained from SeouLin Bioscience (Seoul, Korea). The TNF-α, IL-6 and MCP-1 kit was procured from R&D Systems (Minneapolis, MN, USA). SYTOX green was purchased from Life Technologies (Eugene, OR, USA). Buffers were prepared using Milli-Q ultrapure water (Merck Millipore, Billerica, MA, USA). All other reagents were of analytical grade.

3. Results

3.1 Peptide design and characterization

The Lf-KR hybrid peptide was designed so that LfcinB6 and KR-12-a4 were placed at the N-terminus and C-terminus of the peptide, respectively. The N-terminal segment (LfcinB6) and C-terminal segment (KR-12-a4) were connected by Pro. The key physicochemical parameters of the peptides are listed in Table 1. The theoretical molecular weight of each peptide was confirmed by electrospray ionization-mass spectrometry (ESI-MS) (Fig. S1 and Table 1). The calculated and measured values of all peptide weights were consistent, confirming that the Lf-KR peptide was accurately synthesized. HPLC retention time is an important indicator of the relative hydrophobicity of the peptides. The HPLC retention times of LfcinB6, KR-12-a4, and Lf-KR were 13.056, 18.482, and 23.990 min, respectively (Fig. S2), indicating the following hydrophobic order: Lf-KR > KR-12-a4 > LfcinB6.

3.2 The tertiary structure of the Lf-KR

Three predictive models of the three-dimensional structure of Lf-KR were obtained from the I-TASSER server (http://zhanglab.ccmb.med.umich.edu/I-TASSER/)[29]. Model 1 for Lf-KR with the highest C-score was selected (Fig. 1a). The estimated accuracy of Model 1 for Lf-KR was as follows: C score: -0.27; template modeling TM-score: 0.68 ± 0.12; and root-mean-square deviation (RMSD): 1.4 ±2.4 Å. The confidence (C)-score estimates the quality of the ITASSER predicted models, typically in the range from -5 to 2, where a higher value signifies a model with high confidence. The TM-score is a recently proposed scale that measures the similarity between two structures. A TM-score > 0.5 and < 0.17 indicates a model of correct topology and random similarity, respectively. RMSD is the average distance of all the residue pairs in the two structures. As shown in Fig. 1a, Lf-KR adopts a typical α-helical structure at the C-terminus.

3.3 α-helical wheel plot of Lf-KR

The α-helical wheel plot of Lf-KR was predicted using the online analysis tool, HeliQuest server (https://heliquest.ipmc.cnrs.fr/cgi-bin/ComputParams.py) (Fig. 1b). The results showed that Lf-KR carries a +9 net charge with hydrophobicity of 0.340 and a hydrophobic moment of 0.646 (Table 1). It also has a hydrophobic face consisting of WIWIPLV (Fig. 1b).

3.4 CD spectroscopy

To examine further the secondary structure of the peptides in different environments, CD spectra were measured in mimicking the aqueous environment (10 mM PBS) and in bacterial membrane mimicking environment (50% TFE, 30 mM SDS micelles and EYPC/EYPG (1:1) vesicles). As shown in Fig. 2, except LfcinB6, KR-12-a5, and Lf-KR had a stable α-helical conformation in 50% TFE and 30 mM SDS. They had negative peaks at 208 nm and 222 nm, and a positive peak at 192 nm characteristic of a α-helical structure. In the presence of EYPC/EYPG (1:1) vesicles, only Lf-KR showed an α-helical structure. However, the spectra of all peptides in 10 mM PBS are characteristic of unordered conformations.

3.5 Antimicrobial and hemolytic activities

The antimicrobial activities of the peptides against gram-negative and gram-positive bacteria including antibiotic-resistant bacteria were evaluated by measuring their MICs (Table 2). Except for LfcinB6, all peptides exhibited broad-spectrum antimicrobial activities against a panel of bacteria tested, with MICs ranging from 1 to 64 μM. The geometric mean (GM) of the MIC value of Lf-KR was approximately 6-times lower than that of KR-12-a4. The GM of Lf-KR showed potent antimicrobial activity comparable to melittin that is known to have relatively strong antimicrobial activity among various AMPs. The hemolytic activities of the peptides against sheep red blood cells (sRBCs) were measured to determine their toxicity to mammalian cells (Table 2). All peptides had negligible hemolytic activity even at the highest concentration of 128 μM.

3.6 Cell selectivity (therapeutic index)

The therapeutic index (TI) is defined as the ratio of the minimum hemolytic concentration (MHC) of peptides to the geometric mean (GM) of the peptides (Table 2). TI is an important index for evaluating the clinical application value of antimicrobial agents. Lf-KR had a relatively high TI value of 36.6, approximately 6-fold higher than that of KR-12-a4. This result showed that Lf-KR had greater cell selectivity toward bacterial cells than mammalian cells due to its potent antimicrobial activity and minimal hemolytic activity, indicating that it has greater therapeutic potential. In contrast, as a control peptide, melittin (TI = 0.8) has a very low TI value because of its extremely high hemolytic activity.

3.7 Salt insensitivity

The antimicrobial activities of the peptides were tested following the addition of physiological concentrations of different salts for the sensitivity assay. As indicated in Table 3, Lf-KR retained its antimicrobial activity even at high salt concentrations. However, in the presence of high salt concentrations, KR-12-a4 showed significant antimicrobial activity.

3.8 Cytoplasmic membrane depolarization

A membrane potential-dependent probe ($DiSC_3$-5) was used to evaluate the ability of the peptides to depolarize the bacterial cytoplasmic membrane. When the cytoplasmic membrane is permeable and destroyed, the membrane potential is eliminated and $DiSC_3$-5 is released into the medium, causing an increase in fluorescence[30]. The membrane depolarization induced by the peptides was monitored for 500 s. LfcinB6 did not induce cell membrane depolarization at 2 × MIC (Fig. 3a). Compared with KR-12-a4, Lf-KR showed faster and stronger membrane depolarization (Fig. 3a).

3.9 Dye leakage

As shown in Fig. 3b, LfcinB6 did not induce any dye leakage from the bacterial membrane mimicking EYPE/EYPG (7: 3, v/v) liposomes even at 32 μM. KR-12-a4 reached the maximum dye leakage at 0.5 μM, and no further dye leakage was

observed even at 32 μM. However, Lf-KR increased dye leakage in a dose-dependent manner.

3.10 RAW264.7 cell viability

Before investigating the inhibitory activity against LPS-induced inflammation, the cytotoxicity of the peptides against RAW264.7 was evaluated using the MTT assay. As illustrated in Fig. 4, none of the peptides affected the viability of RAW264.7 cells at concentrations as high as 4 μM. Therefore, assays examining the effects of the peptides on LPS-induced NO and TNF-α production were conducted at a concentration of 4 μM.

3.11 Inhibition effect of the peptides on LPS-induced NO and pro-inflammatory cytokine TNF-α production

LPS, also termed endotoxin, is the main component of the outer membrane of gram-negative bacteria[31]. LPS is an effective agonist of Toll-like receptor 4 (TLR4) on the membrane of many types of immune cells. LPS can induce the release of pro-inflammatory mediators such as nitric oxide (NO) and TNF-α in macrophage cells[32]. The overproduction of pro-inflammatory mediators has been implicated in the pathogenesis of septic shock causing tissue damage and myocardial depression[32-34]. The anti-inflammatory effects of the peptides were evaluated by determining the release of NO and TNF-α from LPS-stimulated RAW264.7 cells (Fig. 5). RAW264.7 cells were stimulated with 200 ng/mL LPS in the presence of 4 μM peptide. NO production was determined by the Griess method that detects nitrite ion (NO_2^-) accumulation in the culture medium (Fig. 5a). The inhibitory effect of the peptides on the release of TNF-α in LPS-stimulated RAW264.7 cells was also investigated using commercially available ELISA kits (Fig. 5b). Compared with LfcinB6 and KR-12-a4, the addition of Lf-KR was more effective at inhibiting NO and TNF-α production. Similar to LL-37, a powerful anti-inflammatory peptide, Lf-KR inhibited both NO and TNF-α production in LPS-stimulated RAW264.7 cells at a concentration of 4 μM (Fig. 5). The mRNA expression levels of iNOS and TNF-α were determined by RT-

PCR. Lf-KR was as effective as LL-37 in suppressing iNOS (inducible nitric oxide synthase) and TNF-α expression (Fig. 6 and Fig.S3). These data are in good agreement with the observed inhibition of the NO and TNF-α release by the peptides.

3.12 LPS-binding activity

We assessed the direct LPS-binding ability of the peptides using a fluorescence-based displacement assay with BODIPY TR cadaverine (BC). Initially, BC fluorescence is quenched when it binds to free LPS. The introduction of antiendotoxin compounds displaces BC, its fluorescence increases, indicating successful binding of the compound with LPS. As shown in Fig. 7, Lf-KR showed a concentration-dependent increase in BC fluorescence intensity, similar to that of LL-37, with almost 100% binding to LPS at 8 μM.

3.13 Anti-biofilm activity

The anti-biofilm activity of the peptides was determined by their ability to eradicate preformed biofilm cells. We used the minimum biofilm eradication concentration (MBEC) to evaluate the anti-biofilm activity of the peptides. As shown in Fig. 8a and Table 5, Lf-KR showed excellent eradication activity with $MBEC_{50}$ and MBEC against the established MDRPA biofilm at concentrations of 8 μM and 32 μM, respectively. In contrast, the MBECs of KR-12-a4 and LfcinB6 were 64 μM and > 64 μM, respectively. Lf-KR exhibited anti-biofilm activity similar to or slightly higher than that of LL-37, known as an anti-biofilm agent (Fig. 8a and Table 5). To demonstrate the anti-biofilm activity of Lf-KR on mature MDRPA biofilms, a laser confocal scanning microscope (CLSM) was used to visualize the preformed MDRPA biofilm after treatment with Lf-KR. The biofilm was grown for 24 h and treated with Lf-KR for 1h followed by staining with the fluorescent dyes SYTO 9 (live) and propidium iodide (PI) (dead) bacteria. Under CLSM, a large number of biofilm bacteria were seen aggregated into the control group, mainly living bacteria with green fluorescence (Fig. 8b). The number of MDRPA biofilm cells decreased significantly after treatment with Lf-KR at MBEC (32 μM) for 24 h. The number of dead cells increased, and only

scattered bacterial aggregates were present in the field of view (Fig. 8b). The CLSM data showed that Lf-KR had a strong damaging effect on the MDRPA strain biofilm. Collectively, our results suggest that Lf-KR has potential as an anti-biofilm agent for the treatment of MDRPA infection.

4. Discussion

Hybridization of two AMPs is an effective way to increase antimicrobial activity or decrease the cytotoxicity of the parental AMPs[35-37]. In this study, a novel hybrid AMP, Lf-KR, was designed by combining the antimicrobial core sequence (LfcinB6) of LfcinB (bovine lactoferricin) and a potent analog (KR-12-a4) of the shortest antimicrobial sequence (KR-12) of human AMP LL-37 and placing a Pro molecular hinge between these two sequences (Table 1).

Consequently, Lf-KR showed remarkably increased antimicrobial activity and cell selectivity against gram-positive and gram-negative bacteria including antibiotic-resistant bacteria compared to LfcinB6 and KR-12-a4, without increasing hemolytic activity (Table 2). It is known that the antimicrobial activity of α-helical amphipathic AMPs is mainly influenced by positive charges and hydrophobicity[38-40]. Previous studies demonstrated that a proper positive charge (usually +6 to +7) was essential for antimicrobial activity, but antimicrobial activity did not increase when the positive charge of AMPs was beyond the threshold[41,42]. In this study, the positive charge of Lf-KR was +9 (Table 1). The HPLC-retention time (RT) typically reflects the hydrophobicity of peptides. Lf-KR (RT: 23.990 min) displayed higher hydrophobicity than KR-12-a4 (RT: 18.482 min) (Table 1 and Fig. S2). Therefore, it is suggested that the enhanced antimicrobial activity of Lf-KR is due to its increased hydrophobicity rather than its increased positive charge.

The therapeutic applications of AMPs lie in their ability to effectively kill bacterial cells without exhibiting significant hemolytic activity. The cytotoxic property is usually conveyed by the therapeutic index, the ratio of the MHC value to the GM value. A high therapeutic index is an indication of two characteristics of the peptides: a high MHC (low hemolysis) and a low MIC (high antimicrobial activity). The therapeutic index of Lf-KR (TI = 36.6) was approximately six times higher than that of KR-12-a4 (TI = 5.9), known to have a relatively high TI value[12].

The secondary structure of Lf-KR predicted by the Heliquest website is a typical α-helical amphipathic molecule divided into two different sides. One side is the hydrophobic surface composed of hydrophobic amino acid residues such as Ile, Val, Ile, and Trp. The other side is the hydrophilic surface composed of positively charged amino acid residues such as Lys and Arg. CD spectroscopy further confirmed the predicted α-helix structure in membrane-like environments such as TFE and SDS micelles (Fig. 2). Despite its slightly lower α-helix content, Lf-KR showed higher antimicrobial activity than KR-12-a4 (Table 2 & 4). Consistent with the findings of other groups[34,43], this result indicates that a higher α-helical content of the peptide is not necessarily accompanied by higher antimicrobial activity.

Furthermore, the three-dimensional structure of Lf-KR was modeled using the website I-TASSER and displayed using PDB Viewer software. As a result of modeling, it was found that Lf-KR has an N-terminal random coil structure and the typical α-helical structure at the C-terminus (Fig. 1a). These results show that the Lf-KR peptide can form an amphiphilic α-helix structure under suitable membrane conditions, suggesting its antimicrobial activity.

Studies have reported that salts present at physiological concentrations can impair the antimicrobial activity of AMPs[43-45]. These salts are thought to antagonize antimicrobial activity by competing with peptides for membrane binding[43-45]. Specifically, monovalent free ions such as Na+ and K+ prevent peptide molecules from binding to the membrane via charge screening effects[43-45]. In the present study, the sensitivity of peptides to salts at physiological concentrations was investigated by monitoring the changes in MIC values. Lf-KR retained antimicrobial activity against *E. coli* and *S. aureus* in the presence of Na^+, K^+, NH^{4+}, Zn^{2+}, Ca^{2+}, and Fe^{3+} (Table 3). This result suggests that cation valence [monovalent (NH_4^+, K^+, Na^+), divalent (Zn^{2+}, Ca^{2+}), and trivalent (Fe^{3+})] had little or no effect on the strength of the antimicrobial activity of Lf-KR. The high net charge (+9) presented by Lf-KR was sufficient to neutralize the charge screening effect induced by the addition of salts, resulting in maintained

antimicrobial activity. This result agrees with previous reports that peptides with higher net charges are less sensitive to salts[34,46]. Lf-KR contains three tryptophan residues. Also, the salt insensitivity of Lf-KR might be due to the bulky side chain of tryptophan that could enhance the affinity of this AMP for the bacterial membrane and contribute to its strong antimicrobial activity in the presence of salts[46].

Most AMPs exhibit antimicrobial activity by destroying bacterial cell membranes through mechanisms ranging from permeabilization to depolarization and transient gaps[47,48]. In the present study, cytoplasmic membrane potential and dye leakage assays were performed to investigate the interaction between the peptides and the cell membrane. The cytoplasmic membrane potential assay indicated that Lf-KR possessed the ability to damage the bacterial cytoplasmic membrane (Fig. 3a). In addition, Lf-KR increased dye leakage via the bacterial membrane, mimicked by EYPE/EYPG (7: 3, v/v) liposomes, in a dose-dependent manner (Fig. 3b). Therefore, the enhanced antimicrobial activity of Lf-KR is due to increased permeabilization and depolarization of microbial membranes. Membrane destruction leading to loss of barrier function results in leakage of cytoplasmic content and cell death.

LPS, a major component of the outer membrane of gram-negative bacteria, can cause inflammation, sepsis, and shock. Following bacterial death under the action of antimicrobial agents, a large amount of LPS detaches from the cells and enters the blood circulation of the body, activates the inflammatory signaling pathway, and releases inflammatory mediators such as NO and TNF-α[49,50]. Numerous AMPs such as LL-37 and indolicidin-derived peptides[23-26] have been described that not only show broad-spectrum antimicrobial activity but also inhibit the release of pro-inflammatory cytokines. In the present study, the anti-inflammatory activity of Lf-KR was investigated and compared with that of LL-37. At non-toxic concentrations, Lf-KR significantly inhibited NO and TNF-α production and their gene expression in LPS-stimulated RAW264.7 cells with a potency equivalent to LL-37 (Fig. 5 and 6). This result suggests that Lf-KR has

the potential to be developed as an anti-inflammatory agent by blocking LPS-mediated inflammatory mediators. The exact mechanism of the anti-inflammatory activity of AMPs in LPS-stimulated RAW264.7 cells is controversial. It is known that one of the possible mechanisms of the anti-inflammatory activity of AMPs is direct interaction with LPS. The BODIPY TR cadaverine (BC) assay demonstrated that the LPS-binding activity of Lf-KR was similar to that of LL-37, known to have powerful LPS-binding activity (Fig. 7). This result suggested that the enhanced anti-inflammatory activity of Lf-KR is due to an increase in the direct interaction with LPS.

Biofilms are considered one of the most resistant mechanisms of bacterial cell survival that cannot be managed by the available conventional antibiotics[27,28]. In general, compared to planktonic cells, biofilms take 10-fold to 1000-fold higher concentrations of traditional antibiotics to be eradicated due to their specific nature of resistance including the extracellular lipopolysaccharide matrix that delays antibiotic penetration and hence leads to the loss of treatment efficiency[27,28]. It is encouraging that AMPs have anti-biofilm activity because of their special mode of action[51,52]. In this study, the ability of Lf-KR to eradicate preformed MDRPA biofilms was evaluated in vitro. Notably, Lf-KR eradicated 100% of mature biofilms at a concentration of 16 μM (Fig. 8a and Table 5). Although the mechanism of action of AMPs against biofilms is not clear, one possible explanation is that AMPs have anti-biofilm activity by forming pores within the lipid components of the biofilm, passing through the extracellular biofilms, or dispersing the biofilms[53,54]. Therefore, CLSM was used to examine mature MDRPA biofilm after treatment with the peptides to visualize the possible biofilm-disruptive activity. Lf-KR disrupted mature MDRPA biofilm as assessed by CLSM (Fig. 8b). Collectively, our results suggest that Lf-KR is a potential bacterial biofilm-eradicating agent for the treatment of mature MDRPA biofilms.

5. Conclusion

In the present study, we developed a novel hybrid AMP, Lf-KR, with enhanced cell selectivity by combining LfcinB6 and KR-12-a4 and introducing a Pro hinge between these two sequences. Lf-KR exerted high cell selectivity for bacterial cells. Lf-KR has broad-spectrum antimicrobial activity against gram-positive and gram-negative bacteria, including several antibiotic-resistant strains, without increasing hemolytic activity. Lf-KR retained its antimicrobial activity in the presence of salts at physiological concentrations. Lf-KR significantly inhibited the expression and production of pro-inflammatory cytokines (NO and TNF-α) in LPS-stimulated mouse macrophage RAW264.7 cells. Lf-KR showed a strong eradication effect on the preformed MDRPA biofilm. It was observed by CLSM that Lf-KR disrupted the structure of the preformed MDRPA biofilm. Collectively, our results suggest that Lf-KR is a putative candidate for the development of antimicrobial, anti-inflammatory, and anti-biofilm agents.

Table 1. Amino acid sequence and physicochemical properties of LfcinB6, KR-12-a4 and Lf-KR

Peptides	Amino acid sequence	Net charge	t_R (min)[a]	µH	Average Mass (Da)	MS Analysis[b]			
						z	m/z calculated		m/z found
LfcinB6	RRWQWR-NH_2	3	13.056	–	987.13	$[M+H]^+$	988.13		987
						$[M+2H]^{2+}$	494.6		493.9
		6	18.482	0.912	1581.06	$[M+H]^+$	1582.06		1580.5
						$[M+2H]^{2+}$	791.5		791.3
						$[M+3H]^{3+}$	528		527.7
KR-12-a4	KRIVKLIKKWLR-NH_2					$[M+2H]^{2+}$	1324.6		1324.3
		9	23.99	0.646	2647.28	$[M+3H]^{3+}$	883.4		883.4
						$[M+4H]^{4+}$	662.8		662.8
Lf-KR	RRWQWRPKRIVKLIKKWLR-NH_2								

[a] Retention times (t_R) were determined by analytical RP-HPLC on a C_{18} column (5 mm; 4.6 mm ′ 250 mm; Vydac) using a gradient of buffer B (0.05% TFA in CH_3CN/H_2O 90:10 v/v) in buffer A (0.05 %TFA in H_2O) for 60 min with a flow rate of 1.0 mL/min.

[b] mH: Hydrophobic moment

[c] Molecular masses were determined by electrospray ionization mass spectrometry (ESI-MS). z: ion charge, m/z: mass-to-charge ratio

Table 2. MIC, MHC and TI of LfcinB6, KR-12-a4 and Lf-KR against different bacterial strains

Bacterial strains	MIC [a] (mM)			
	LfcinB6	KR-12-a4	Lf-KR	Melittin
Gram-positive bacteria				
S. aureus (KCTC 1621)	>64	16	4	4
S. epidermidis (KCTC 1917)	>64	16	8	4
B. subtilis (KCTC 3068)	>64	4	4	4
Resistant Gram (+) bacteria				
MRSA[e] (CCARM 3089)	>64	64	8	4
MRSA (CCARM 3090)	>64	>64	8	4
MRSA (CCARM 3095)	>64	>64	8	8
VREF[f] (ATCC 51559)	>64	64	8	4
Gram-negative bacteria				
E. coli (KCTC 1682)	>64	16	8	4
P. aeruginosa (KCTC 1637)	>64	8	8	16
S. typhimurium (KCTC 1926)	>64	8	4	4
Resistant Gram (-) bacteria				
MDRPA[g] (CCARM 2095)	>64	4	8	8
MDRPA (CCARM 2109)	>64	64	8	8
GM[b] (mM)	>64	43.3	7	6
MHC[c] (mM)	>128	>128	>128	5
TI[d] (MHC/GM)	0.5	5.9	36.6	0.8

[a] Minimum inhibitory concentrations (MICs) were determined as the lowest concentration of the peptides that inhibited bacterial growth.

[b] The geometric mean (GM) of the peptide MICs against the tested bacterial strains was calculated. When no antimicrobial activity was observed at 64 μM, a value of 128 μM was used to calculate the therapeutic index.

[c] MHC is the minimum hemolytic concentration that causes 10 % hemolysis of sheep red blood cells (sRBCs). When no detectable hemolytic
activity was observed at 128 μM, a value of 256 μM was used to calculate the therapeutic index.

[d] Therapeutic index (TI) is the ratio of MHC to GM. Larger values indicate greater cell selectivity.

[e] MRSA: methicillin-resistant *Staphylococcus aureus*

[f] VREF: vancomycin-resistant *Enterococcus faecium.*

[g] MDRPA: multidrug-resistant *Pseudomonas aeruginosa.*

Table 3. Minimum inhibitory concentration (MIC) values of LfcinB6, KR-12-a4 and Lf-KR in the presence of physiological salts against *E. coli* and *S. aureus*

Peptides	Peptide alone	150 mM NaCl	4.5 mM KCl	6 mM NH_4Cl	1 mM $MgCl_2$	2.5 mM $CaCl_2$	4 mM $FeCl_3$
MIC (mM) against *E. coli* (KCTC 1682)							
LfcinB6	>64	>64	>64	>64	>64	>64	>64
KR-12-a4	16	32	16	32	32	32	32
Lf-KR	8	16	8	8	16	16	8
MIC (mM) against *S. aureus* (KCTC1621)							
LfcinB6	>64	>64	>64	>64	>64	>64	>64
KR-12-a4	16	32	>32	>32	>32	>32	>32
Lf-KR	4	4	8	8	8	8	8

Table 4. Mean residual ellipticity at 222 nm ($[q]_{222}$) and percent a-helical contents of LfcinB6, KR-12-a4 and Lf-KR in aqueous buffer, 50% TFE, 30mM SDS and EYPC/EYPG (1:1) vesicles.

	Buffer		50 % TFE		30mM SDS		EYPC/EYPG (1:1)	
Peptide	$[q]_{222}$	% α-helix	$[q]_{222}$	% α-helix	$[q]_{222}$	% α-helix	$[q]_{222}$	% α-helix
LfcinB6	1446.6	rc	-1073.2	rc	1071.2	rc	1405.1	rc
KR-12-a4	-1619.9	rc	-12483.8	28.74	-11431.6	25.55	-3430	rc
Lf-KR	-1538.6	rc	-10967.4	24.14	-10534.3	22.83	-7843.2	14.68

% α-helix = $-100\ ([q]_{222} + 3000)/33000$. rc means random coil.

Table 5. Minimum biofilm eradication concentration (MBEC) of LfcinB6, KR-12-a4, Lf-KR and LL-37.

Peptides	$MBEC_{50}$ (μM)	$MBEC_{90}$ (μM)	MBEC (μM)
LfcinB	>64	>64	>64
KR-12-a4	64	64	64
Lf-KR	8	16	32
LL-37	16	32	32

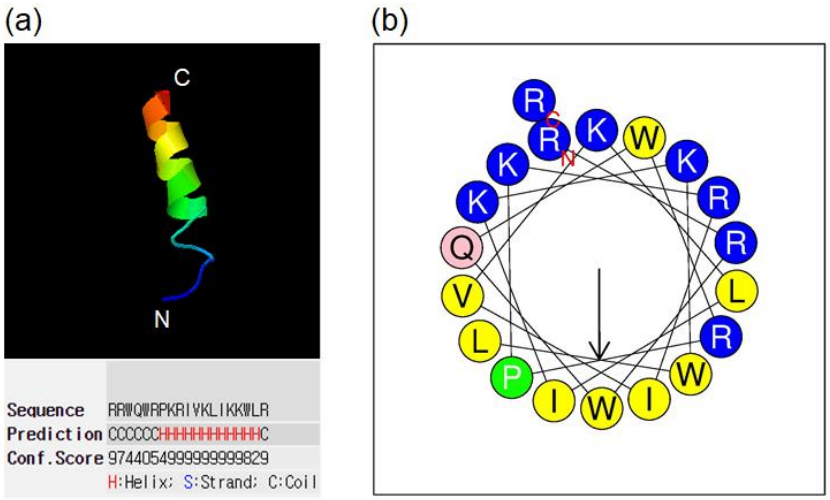

Figure 1. (a) Tertiary structure and (b) α-helical wheel plot of hybrid peptide Lf-KR predicted by automated I-TASSER server (http://zhanglab.ccmb.med.umich.edu/I-TASSER/) and HeliQuest server (https://heliquest.ipmc.cnrs.fr/cgi-bin/ComputParams.py), respectively. In the α-helical-wheel plot, residues marked in blue and yellow represent positively charged amino acids and hydrophobic amino acids, respectively.

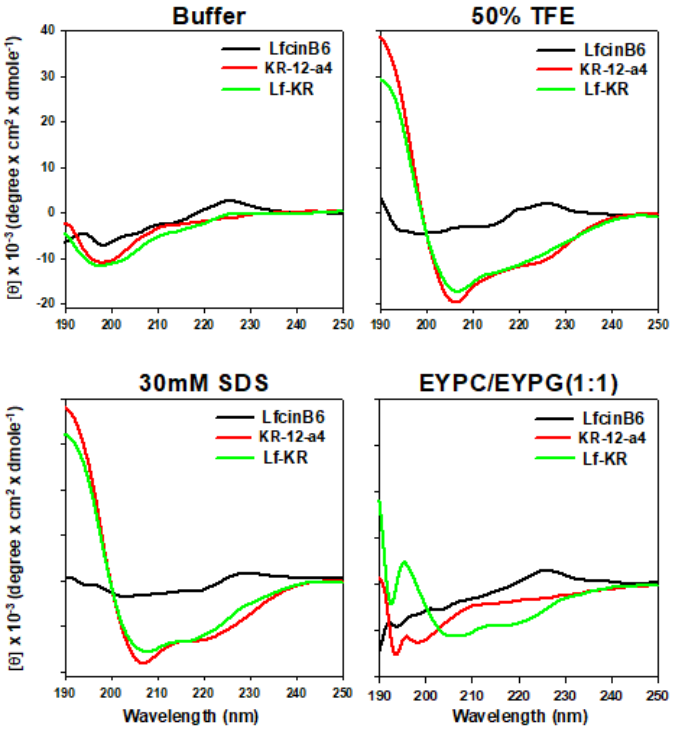

Figure 2. CD (circular dichroism) spectra of LfcinB6, KR-12-a5, and Lf-KR. The mean residue ellipticity was plotted against wavelength. The values from three scans were averaged per sample.

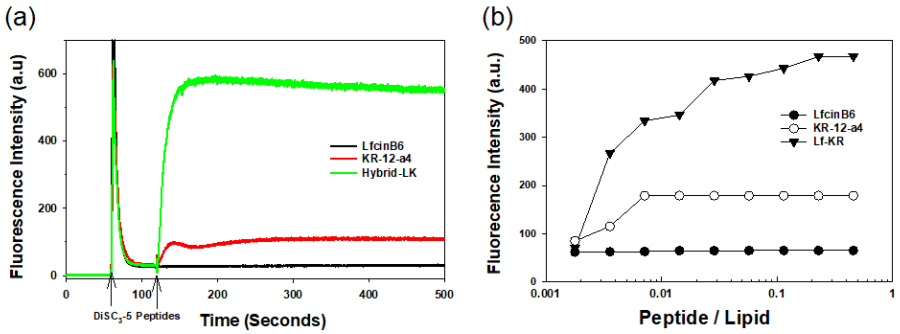

Figure 3.(a) Time-dependent cytoplasmic membrane depolarization of *Staphylococcus aureus* (KCTC 1621) treated with the peptides (2 × MIC) assessed by the release of the membrane potential-sensitive dye, $DiSC_3$-5. (b) Membrane permeabilization caused by the peptides. Dose-dependent calcein release from EYPE/PYPG (7:3) LUVs induced by LfcinB6, KR-12-a5, and Lf-KR. The fluorescence intensity was measured using an excitation wavelength of 490 nm and an emission wavelength of 520 nm.

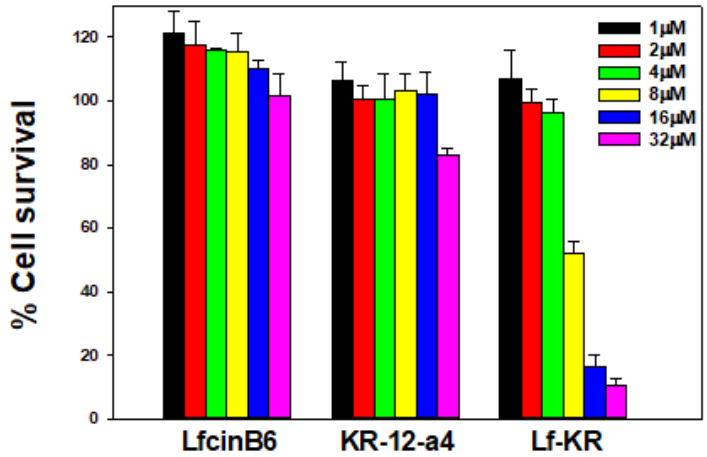

Figure 4. Cytotoxicity of LfcinB6, KR-12-a5, and Lf-KR against mouse macrophage RAW264.7 cells.

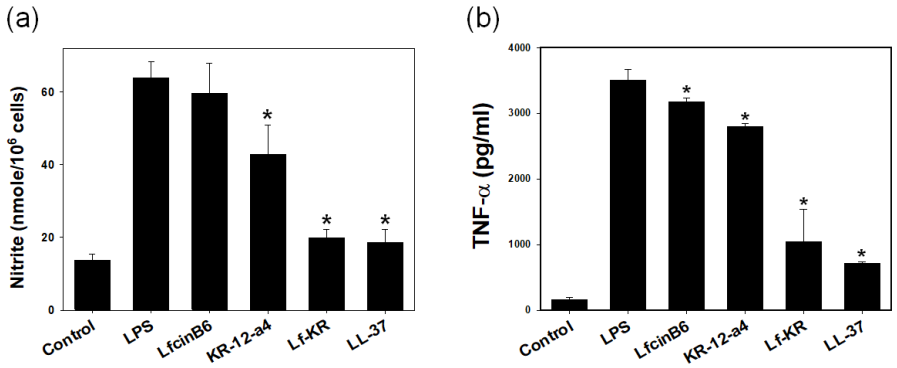

Figure 5. (a) Effects of LfcinB6, KR-12-a5, Lf-KR, and LL-37 on nitric oxide (NO) production in LPS-stimulated RAW264.7 cells. (b) Effects of LfcinB6, KR-12-a5, and Lf-KR on TNF-α release from LPS-stimulated RAW264.7 cells. All data represent at least three independent experiments and are expressed as mean ± standard error of the mean (SEM). Data were analyzed by one-way ANOVA with Bonferroni's post-test. Asterisks indicate statistically significant differences (*P < 0.001 for each agonist). Results were similar when the experiments were repeated using different cells. Peptide concentration is 4 μM.

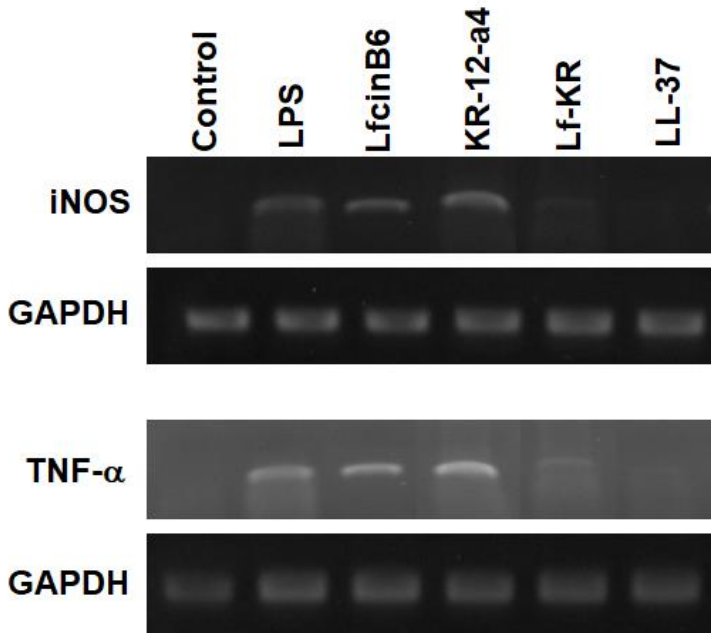

Figure 6. Effects of LfcinB6, KR-12-a5, Lf-KR, and LL-37 on the mRNA levels of iNOS and TNF-α in LPS-stimulated RAW264.7 cells. RAW264.7 cells (5×105 cells/well) were incubated with the peptides in the presence of LPS (20 ng/mL) for 3 h (for TNF-α) or 6 h (for iNOS). Total RNA was isolated and analyzed to determine the levels of iNOS and TNF-α mRNAs by RT-PCR.

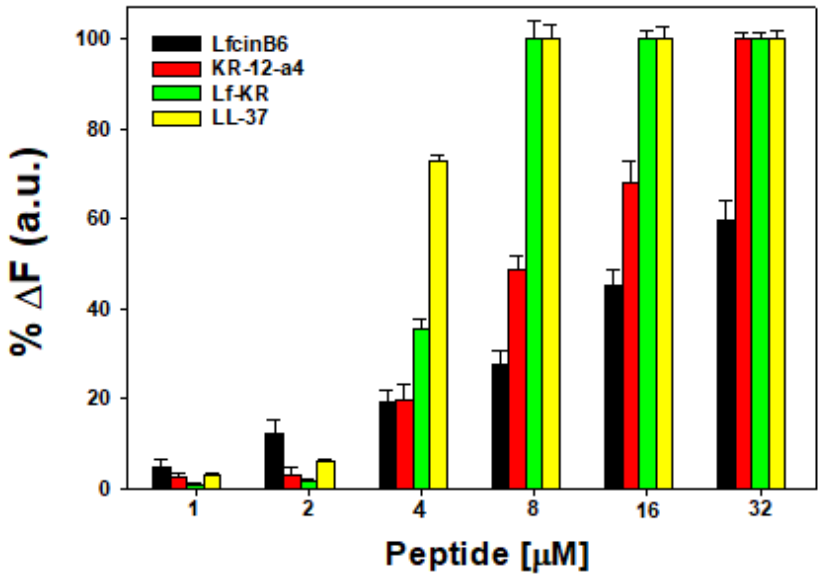

Figure 7. The binding ability of LfcinB6, KR-12-a5, Lf-KR, and LL-37 to LPS from E. coli 0111:B4. The fluorescence intensity was monitored at an excitation wavelength of 580 nm and an emission wavelength of 620 nm.

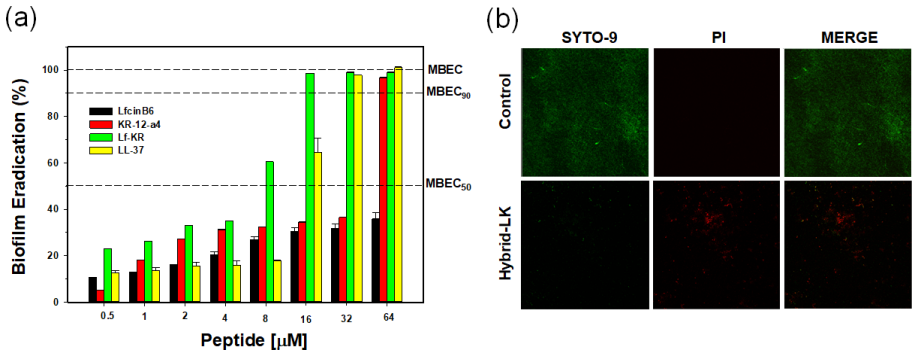

Figure 8. (a) Biofilm eradication activity of LfcinB6, KR-12-a5, Lf-KR and LL-37 against multidrug-resistant *Pseudomonas aeruginosa* (MDRPA). The dotted lines indicate 50% and 90% eradication concentrations. (b) Effects of Lf-KR on MDRPA mature biofilms were assessed using confocal laser scanning microscopy (CLSM). MDRPA were incubated alone or with Lf-KR (16 μM). Biofilms were visualized with live–dead viability staining (SYTO 9/PI). The viable cells exhibited green fluorescence (SYTO 9), whereas the dead cells exhibited red fluorescence (PI).

References

[1] Rossolini, G. M., Arena, F., Pecile, P. & Pollini, S. Update on the antibiotic resistance crisis. *Curr. Opin. Pharmacol.* **18**, 56–60 (2014).

[2] Zhang, L. J. & Gallo, R. L. Antimicrobial peptides. *Cur. Biol.* **26**, R14–19 (2016).

[3] Pasupuleti, M., Schmidtchen, A. & Malmsten, M. Antimicrobial peptides: key components of the innate immune system. *Crit. Rev. Biotechnol*. **32**, 143–171 (2012).

[4] Andreu, D. et al. Shortened cecropin A-melittin hybrids significant size reduction retains potent antibiotic activity. *FEBS Lett.* **296**, 190–194 (1992).

[5] Boman, H. G., Wade, D., Boman, L. A., Wihlin, B. & Merrifield, R.B. Antibacterial and antimalarial properties of peptides that are cecropin-melittin hybrids. *FEBS Lett.* **259**, 103–106 (1989).

[6] Liu, Y. F., Xia, X., Xu, L. & Wang, Y. Z. Design of hybrid -hairpin peptides with enhanced cell specificity and potent anti-inflammatory activity. *Biomaterials* **34**, 237–250 (2013)

[7] Dong, N. et al. Characterization of bactericidal efficiency, cell selectivity, and mechanism of short interspecific hybrid peptides. *Amino Acids* **50**, 453–468 (2018)

[8] Bellamy, W. et al. Identification of the bactericidal domain of lactoferrin. *Biochim. Biophys. Acta-Biomembr*. **1121**, 130–136 (1992).

[9] Schibli, D. J., Hwang, P. M. & Vogel, H. J. The structure of the antimicrobial active center of lactoferricin B bound to sodium dodecyl sulfate micelles. *FEBS Lett.* **446**, 213–217 (1999).

[10] Richardson, A., de Antueno, R., Duncan, R. & Hoskin, D. W. Intracellular delivery of bovine lactoferricin's antimicrobial core (RRWQWR) kills T-leukemia cells. *Biochem. Biophys. Res. Commun*. **388**, 736–741 (2009).

[11] Wang, G. et al. Structures of human host defense cathelicidin LL-37 and its smallest antimicrobial peptide KR-12 in lipid micelles. *J. Biol. Chem.* **283**, 32637–32643 (2008).

[12] Jacob, B., Park, I. S., Bang, J. K. & Shin, S. Y. Short KR-12 analogs designed from human cathelicidin LL-37 possessing both antimicrobial and antiendotoxic activities without mammalian cell toxicity. *J. Pept. Sci.* **19**, 700–707 (2013).

[13] Song, Y. M. et al. Effects of L- or D-Pro incorporation into hydrophobic helix or hydrophilic helix face of amphipathic α-helical model peptide on structure and cell selectivity. *Biochem. Biophys. Res. Commun.* **314**, 615–621 (2004).

[14] Suh, J. Y. et al. Structural and functional implications of a proline residue in the antimicrobial gaegurin. *Eur. J. Biochem.* **266**, 665–674 (1999).

[15] Lee, J. K. et al. A proline-hinge alters the characteristic of the amphipathic α-helical AMPs.*PLoS One.* **8**, e67597 (2013).

[16] Tieleman, D. P., Shrivastava, I. H., Ulmschneider, M. R. & Sansom, M. S. Proline-induced hinges in transmembrane helices: possible role in ion channel gating. *Proteins* **44**, 63–72 (2001)

[17] Pukala, T. L., Brinkworth, C. S., Carver, J. A. & Bowie, J. H. Investigating the importance of the flexible in caerin 1.1: solution structure and activity of two synthetically modified caerin peptides. *Biochemistry* **43**, 937–944 (2004)

[18] Park, C. B., Yi, K. S., Matsuzaki, K., Kim, M. S. & Kim. S. C. Structure-activity analysis of buforin II, a histone H2A derived antimicrobial peptide: the proline hinge is responsible for the cell-penetrating activity of buforin II. *Proc. Natl. Acad. Sci. U.S.A.* **97**, 8245–8250 (2000).

[19] Park, J. M., Jung. J. E. & Lee, B. J. Antimicrobial peptides from the skin of a Korean frog, Rana rugosa. *Biochem. Biophys. Res. Commun.* **218**, 408–413 (1994)

[20] Lee, S. A. et al. Solution structure and cell selectivity of piscidin 1 and its analogues. *Biochemistry*, **46**, 3653-3663 (2007)

[21] Yang, S. et al. Possible role of s PXXP central hinge in the bacterial activity and membrane interaction of PMAP-23, a member of cathelicidin family. *Biochemistry*, **45**, 3653–3663 (2006)

[22] Yang, S., Shin, S. Y. & Shin, S. The central PXXP motif is crucial for PMAP-23 translocation across the lipid bilayer. *Int. J. Mol. Sci.* **22**, 9752 (2021)

[23] Mookherjee, N. K. L. et al. Modulation of the TLR-mediated inflammatory response by the endogenous human host defense peptide LL-37. *J. Immunol.* **176**, 2455–2464 (2006).

[24] Nan, Y. H. et al. Investigating the effects of positive charge and hydrophobicity on the cell selectivity, mechanism of action and anti-inflammatory activity of a .Trp-rich antimicrobial peptide indolicidin. *FEMS Microbiol. Lett.* **292**, 134–140 (2009)

[25] Nagaoka, I. et al. Cathelicidin family of antibacterial peptides CAP18 and CAP11 inhibit the expression of TNF-α by blocking the binding of LPS to CD14(+) cells. *J. Immunol.* **167**, 3329–3338 (2001).

[26] Nan, Y. H., Bang, J. K. & Shin, S. Y. Design of novel indolicidin-derived antimicrobial peptides with enhanced cell specificity and potent anti-inflammatory activity. *Peptides* **30**, 832–838 (2009).

[27] Costerton, J. W., Stewart, P. S. & Greenberg, E. P. Bacterial biofilms: a common cause of persistent infections. *Science* **284**, 1318–1322 (1999).

[28] O'Toole, G., Kaplan, H. B. & Kolter, R. Biofilm formation as microbial development. *Annu. Rev. Microbiol.* **54**, 49–79 (2000).

[29] Zhang, Y. I-TASSER server for protein 3D structure prediction. *BMC Bioinformatics*. **9**, 40 (2008).

[30] Chou, S. et al. Short, multiple-stranded β-hairpin peptides have antimicrobial potency with high selectivity and salt resistance. *Acta Biomater.* **30**, 78–93 (2016).

[31] Tan, Y. & Kagan, J. C. A cross-disciplinary perspective on the innate immune responses to bacterial lipopolysaccharide. *Mol. Cell* **54**, 212−223 (2014).

[32] Cobb, J. P. & Danner, R. L. Nitric oxide and septic shock. *JAMA* **275**, 1192–1196 (1996).

[33] Scott, M. G., Vreugdenhil, A. C., Buurman, W. A., Hancock, R. E. & Gold, M. R. Cutting edge: cationic antimicrobial peptides block the binding of lipopolysaccharide (LPS) to LPS binding protein. *J. Immunol.* **164**, 549–553 (2000).

[34] Ma, Z. et al. Characterization of cell selectivity, physiological stability and endotoxin neutralization capabilities of α-helix-based peptide amphiphiles. *Biomaterials* **52**, 517–530 (2015).

[35] Shin, A. et al. Peptoid-substituted hybrid antimicrobial peptide derived from papiliocin and magainin 2 with enhanced bacterial selectivity and anti-inflammatory activity. *Biochemistry* **54**, 3921–3931 (2015).

[36] Memariani, H. et al. Design and characterization of short hybrid antimicrobial peptides from pEM-2, mastoparan-VT1, and mastoparan-B. *Chem. Biol. Drug Des.* **89**, 327–338 (2017).

[37] Liu, Y. F., Xia, X., Xu, L. & Wang, Y. Z. Design of hybrid β-hairpin peptides with enhanced cell specificity and potent anti-inflammatory activity. *Biomaterials* **34**, 237–250 (2013).

[38] Mattei, B., Miranda, A., Perez, K. R. & Riske, K. A. Structure–activity relationship of the antimicrobial peptide gomesin: The role of peptide hydrophobicity in its interaction with model membranes. *Langmuir* **30**, 3513–3521 (2014).

[39] Chen, Y. et al. Role of peptide hydrophobicity in the mechanism of action of α-helical antimicrobial peptides. *Antimicrob. Agents Chemother.* **51**, 1398–1406 (2007).

[40] Wang, J. J. et al. High specific selectivity and membrane-active mechanism of the synthetic centrosymmetric α-helical peptides with Gly-Gly pairs. *Sci. Rep.* **5**, 15963 (2015).

[41] Shao, C. X. et al. Central β-turn increases the cell selectivity of imperfectly amphipathic α-helical peptides. *Acta Biomater.* **69**, 243–255 (2018).

[42] Yin, L. M. et al. Roles of hydrophobicity and charge distribution of cationic antimicrobial peptides in peptide-membrane interactions. *J. Biol. Chem.* **287**, 7738–7745 (2012)

[43] Zhu, X. et al. Characterization of antimicrobial activity and mechanisms of low amphipathic peptides with different helical propensity. *Acta Biomater.* **18**, 155–167 (2015).

[44] Zhu, X. et al. Design of imperfectly amphipathic α-helical antimicrobial peptides with enhanced cell selectivity. *Acta Biomater.* **10**, 244–257 (2014).

[45] Huang, J. et al. Inhibitory effects and mechanisms of physiological conditions on the activity of enantiomeric forms of an α-helical antibacterial peptide against bacteria. *Peptides* **32**, 1488–1495 (2011).

[46] Saravanan, R. et al. Design of short membrane selective antimicrobial peptides containing tryptophan and arginine residues for improved activity, salt-resistance and biocompatibility. *Biotechnol. Bioeng.* **111**, 37–49 (2014).

[47] Juba, M. L. et al. Helical cationic antimicrobial peptide length and its impact on membrane disruption. *Biochim. Biophys. Acta-Biomembr.* **1848**, 1081–1091 (2015).

[48] Zhu, X. et al. Bactericidal efficiency and modes of action of the novel antimicrobial peptide T9W against Pseudomonas aeruginosa. *Antimicrob. Agents Chemother.* **59**, 3008–3017 (2015).

[49] Cohen, J. et al. Sepsis: A roadmap for future research. *Lancet Infect. Dis.* **15**, 581–614 (2015).

[50] Zong, X. et al. LFP-20, a porcine lactoferrin peptide, ameliorates LPS-induced inflammation via the MyD88/NF-κB and MyD88/MAPK signaling pathways. *Dev. Comp. Immunol.* **52**, 123–131 (2015).

[51] de Breij, A. et al. The antimicrobial peptide SAAP-148 combats drug-resistant bacteria and biofilms. *Sci. Transl. Med.* **10**, 4044 (2018).

[52] Chung, P. Y. & Khanum, R. Antimicrobial peptides as potential anti-biofilm agents against multidrug-resistant bacteria. *J. Microbiol. Immunol.* **50**, 405−410 (2017).

[53] Park, S. C., Park, Y. & Hahm, K. S. The role of antimicrobial peptides in preventing multidrug-resistant bacterial infections and biofilm formation. *Int. J. Mol. Sci.* **12**, 5971–5992 (2011).

[54] Chung, P. Y. & Khanum, R. Antimicrobial peptides as potential anti-biofilm agents against multidrug-resistant bacteria. *J. Microbiol. Immunol. Infect.* **50**, 405–410 (2017).

[55] Kumar, S. D. & Shin, S. Y. Antimicrobial and anti-inflammatory activities of short dodecapeptides derived from duck cathelicidin: Plausible mechanism of bactericidal action and endotoxin neutralization. *Eur. J. Med. Chem.* **204**, 112580 (2020)

[56] White, P. D. & Chan, W. C. Fmoc solid phase peptide synthesis: A practical approach; Eds.; Oxford University Press: New York (2000)

[57] Stromstedt, A. A. et al. Evaluation of strategies for improving proteolytic resistance of antimicrobial peptides by using variants of EFK17, an internal segment of LL-37. *Antimicrob. Agents Chemother*. **53**, 593–602 (2009).

[58] Dong, N. et al. Strand length-dependent antimicrobial activity and membrane-active mechanism of arginine-and valine-rich β-hairpin-like antimicrobial peptides. *Antimicrob. Agents Chemother*. **56**, 2994–3003 (2012).

[59] Jantaruk, P., Roytrakul, S., Sitthisak, S. & Kunthalert, D. Potential role of an antimicrobial peptide, KLK in inhibiting lipopolysaccharide-induced macrophage inflammation. *PloS One* **12**, e0183852 (2017).

[60] Wood, S. J., Miller, K. A. & David, S. A. Anti-endotoxin agents. 1. Development of a fluorescent probe displacement method optimized for the rapid identification of lipopolysaccharide-binding agents. *Comb. Chem. High Throughput Screen.* **7**, 239–249 (2004).

[61] Wood, S. J., Miller, K. A. & David, S. A. Anti-endotoxin agents. 2. Pilot high-throughput screening for novel lipopolysaccharide-recognizing motifs in small molecules. *Comb. Chem. High Throughput Screen.* **7**, 733–747 (2004).

[62] Harrison, J. J. et al. Microtiter susceptibility testing of microbes growing on peg lids: a miniaturized biofilm model for high throughput screening. *Nat. Protoc*. **5**, 1236−1254 (2010).

[63] Basak, A. et al. Antimicrobial peptide-inspired NH125 analogues: bacterial and fungal biofilm-eradicating agents and rapid killers of MRSA persisters.*Org. Biomol. Chem.* **15**, 5503−5512 (2017).

Supplement data

Peptide name	Calculated Mw	$[M+H]^+$	$[M+2H]^{2+}$	$[M+3H]^{3+}$	$[M+4H]^{4+}$
LfcinB6	987.13	988.13	494.6	330.04	247.8

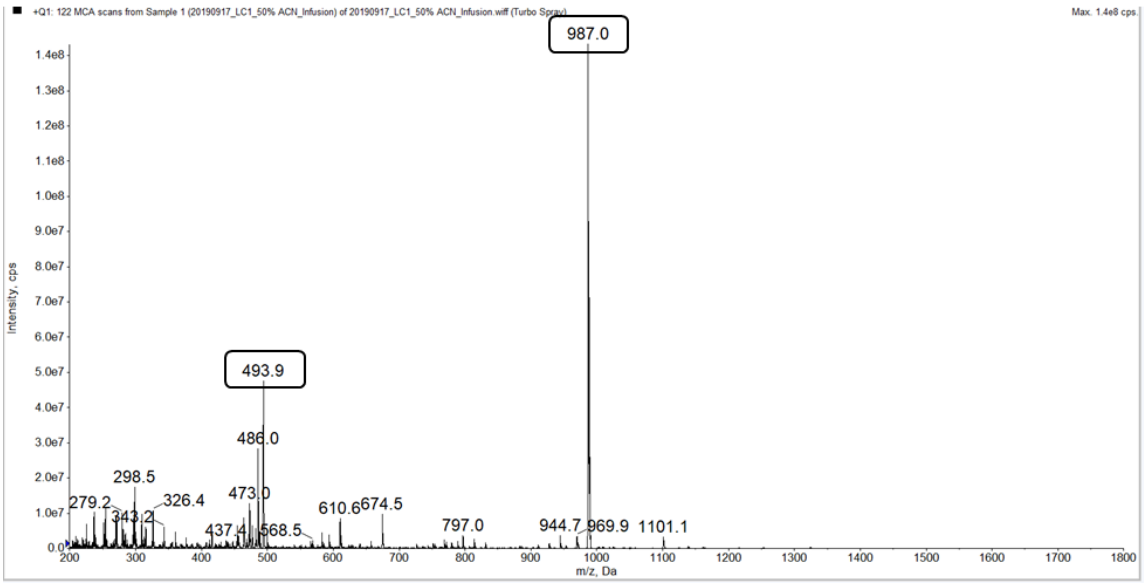

Peptide name	Calculated Mw	$[M+H]^+$	$[M+2H]^{2+}$	$[M+3H]^{3+}$	$[M+4H]^{4+}$
KR-12-a4	1581.06	1582.06	791.5	528.0	396.3

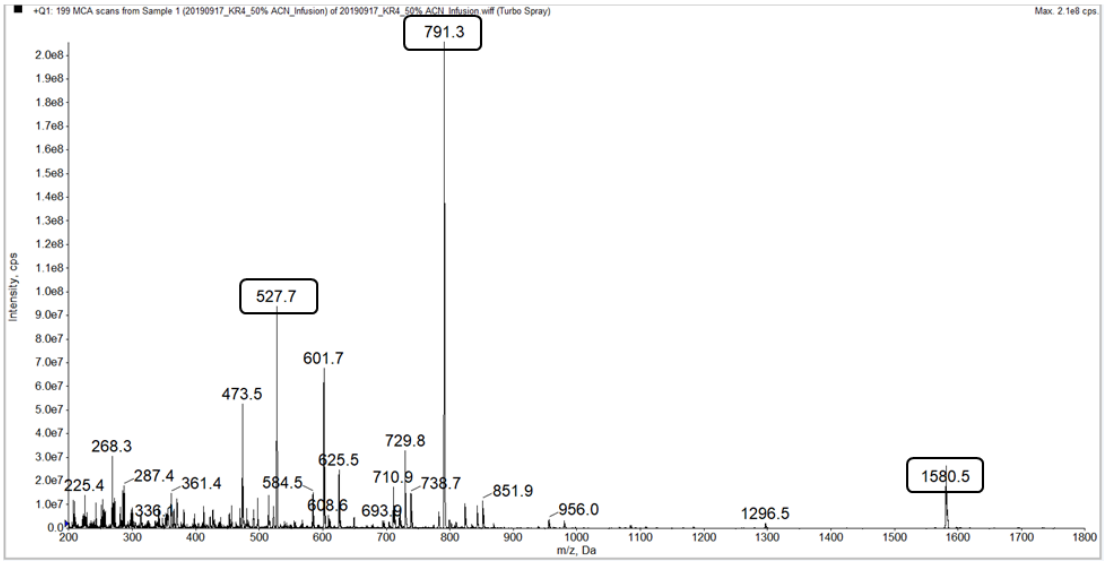

Peptide name	Calculated Mw	$[M+H]^+$	$[M+2H]^{2+}$	$[M+3H]^{3+}$	$[M+4H]^{4+}$
Lf-KR	2647.28	2648.28	1324.6	883.4	662.8

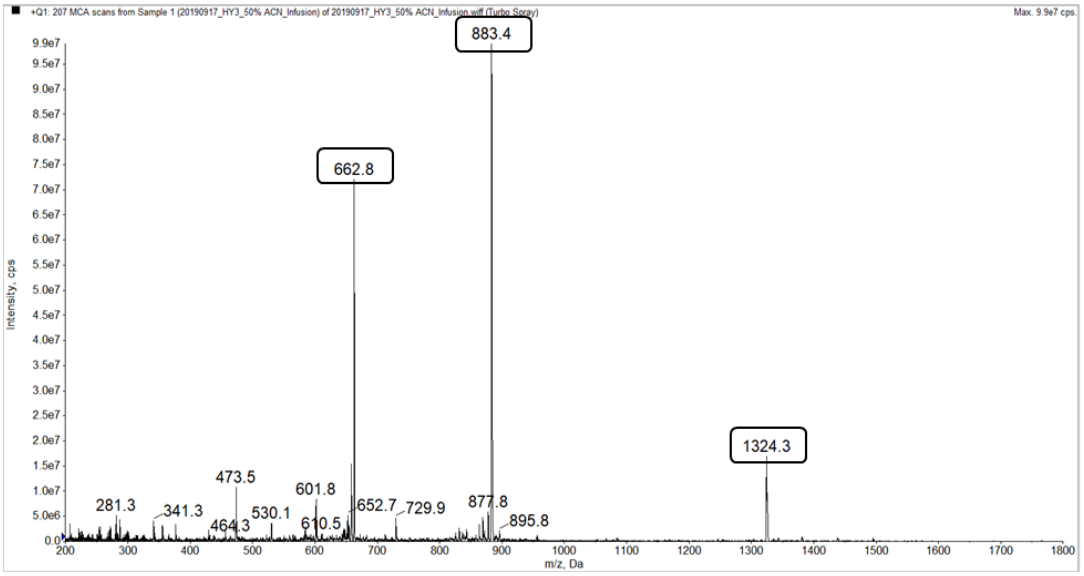

Fig. S1. Molecular masses of synthetic peptides (LfcinB6, KR-12-a4 and Lf-KR) were determined by electrospray ionization-mass spectrometry (ESI-MS).

==== Shimadzu LCsolution Analysis Report ====

Sample Name	: Lfcin B6
Injection Volume	: 20 uL
Data File Name	: LfcinB6.lcd
Method File Name	: small-ka.lcm
Report File Name	: Default.lcr
Data Acquired	: 2021-11-05 오후 3:48:28
Data Processed	: 2021-11-08 오후 6:27:16

<Chromatogram>

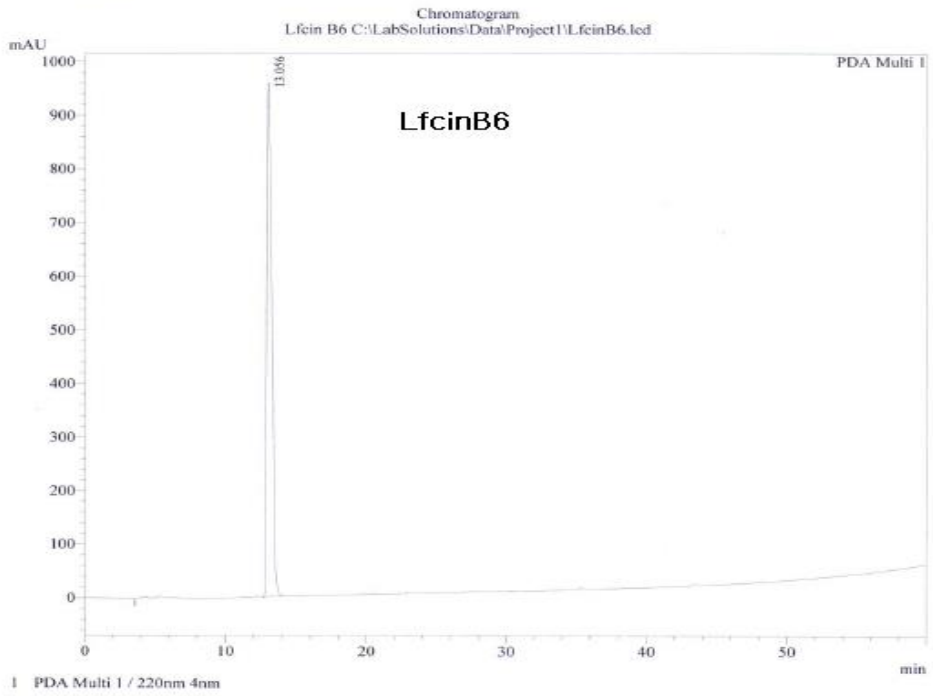

<Results>

PDA Ch1 220nm 4nm

Peak #	Ret. Time	Area	Height	Area %	Height %	Mark
1	13.056	25138429	952325	100.000	100.000	
Total		25138429	952325	100.000	100.000	

==== Shimadzu LCsolution Analysis Report ====

Sample Name	: KR-12-a4
Injection Volume	: 20 uL
Data File Name	: KR-12-a4.lcd
Method File Name	: small-ka.lcm
Report File Name	: Default.lcr
Data Acquired	: 2021-11-08 오후 4:34:27
Data Processed	: 2021-11-08 오후 5:34:29

<Chromatogram>

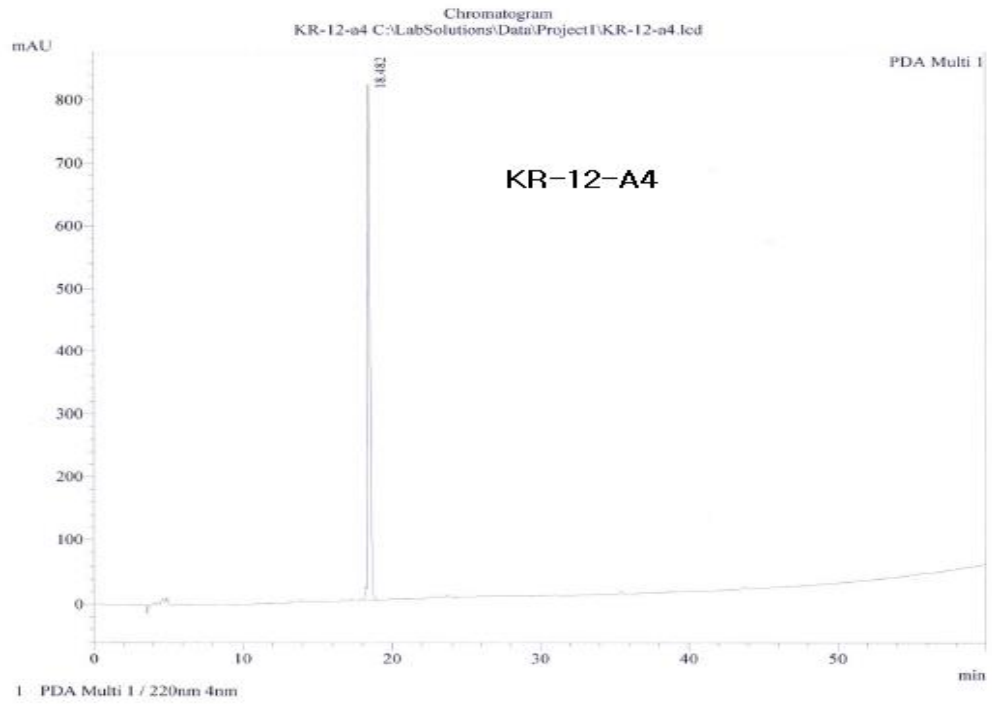

<Results>

PDA Ch1 220nm 4nm

Peak #	Ret. Time	Area	Height	Area %	Height %	Mark
1	18.482	9148695	812124	100.000	100.000	
Total		9148695	812124	100.000	100.000	

==== Shimadzu LCsolution Analysis Report ====

Sample Name	: Hybrid-Lk
Injection Volume	: 20 uL
Data File Name	: Lf-KR.lcd
Method File Name	: small-ka.lcm
Report File Name	: Default.lcr
Data Acquired	: 2021-11-08 오전 11:21:45
Data Processed	: 2021-11-08 오후 6:17:55

<Chromatogram>

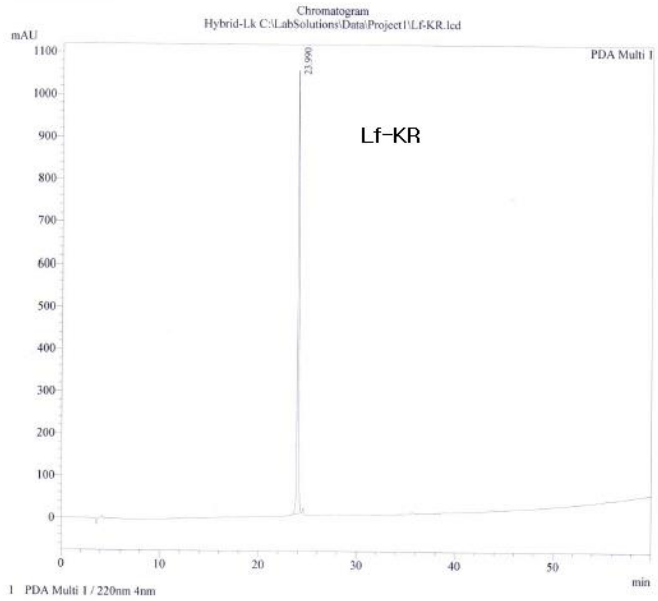

<Results>

PDA Ch1 220nm 4nm

Peak #	Ret. Time	Area	Height	Area %	Height %	Mark
1	23.990	11258080	1037160	100.000	100.000	
Total		11258080	1037160	100.000	100.000	

Fig. S2. Analytical RP-HPLC profiles of synthetic peptides (LfcinB6, KR-12-a4 and Lf-KR). Peptides were eluted for 60 min with a flow rate of 1.0 mL/min by analytical RP-HPLC on a C_{18} column (5 mm; 4.6 mm × 250 mm; Vydac) using a gradient of buffer B (0.05% TFA in CH_3CN/H_2O 90:10 v/v) in buffer A (0.05 %TFA in H_2O).

(a)

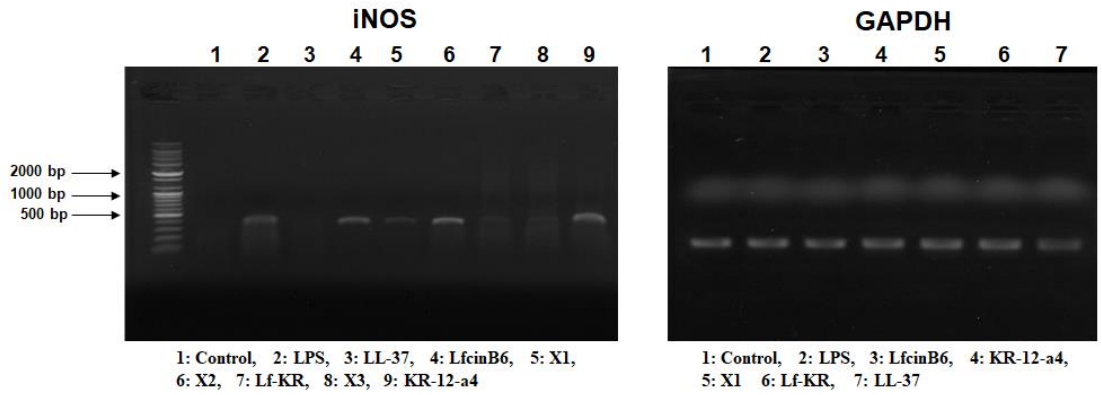

(b)

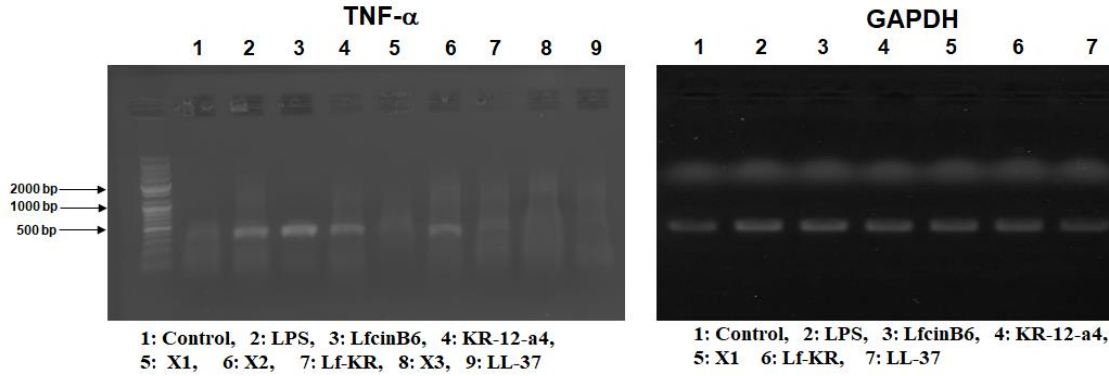

Fig. S3. Effects of LfcinB6, KR-12-a5, Lf-KR, and LL-37 on the mRNA levels of iNOS (a) and TNF-α (b) in LPS-stimulated RAW264.7 cells.

List of pubications

1. **Ajish C**, Yang S, Kumar SD, Shin SY. Proadrenomedullin N-terminal 20 peptide (PAMP) and its C-terminal 12-residue peptide, PAMP (9–20): Cell selectivity and antimicrobial mechanism. **Biochemical and Biophysical Research Communications**. 2020 Jun 30;527(3):744-50.

2. **Ajish C**, Yang S, Kumar SD, Kim EY, Min HJ, Lee CW, Shin SH, Shin SY. A novel hybrid peptide composed of LfcinB6 and KR-12-a4 with enhanced antimicrobial, anti-inflammatory and anti-biofilm activities. **Scientific reports**. 2022 Mar 14;12(1):1-4..

3. Kim EY, Kumar SD, **Ajish C**, Lee CW, Shin SH, Yang S, Bang JK, Shin SY. Synergistic antimicrobial activity of TZP4 with conventional antibiotics against antibiotic-resistant Pseudomonas aeruginosa. **Bulletin of the Korean Chemical Society**. 2022 Mar 18.

ACKNOWLEDGEMENTS

I would first like to thank my thesis advisor, **Professor. Song Yub Shin** for guiding, supporting, understanding, encouraging & invaluable advice throughout the duration of this study and the preparation of this thesis. The door to Prof. Shin's office was always open whenever I faced trouble or had questions about my research or writing. He gave me necessary freedom and consistent support to complete my research projects.

I acknowledge my collaborators, **Prof. Jeong-Kyu Bang** and **Prof. Chul Won Lee** with whom I have many publications. Lots of thanks to my Friend **Dr. Dinesh kumar**, for teaching me all the experiments, clearing my silly doubts. We had endless discussions about various things from chemistry to galaxies and milky ways. I always admire his knowledge and passion towards science. I am lucky to have him in my Ph.D. life.

I would like to express my appreciation to **Dr. Dinesh kumar, Dr. Eun Young Kim** and **Naveen kumar** for helping me in various lab experiments and for making the lab environment lively. Many thanks to the other lab members and collaborators

Foremost I am thankful to my beloved parents, **Chelladurai** and **Jaya Rani**, for raising me, for bearing with me during the challenges and for never having anything but trust in me. They made sure that I concentrate on my studies while they had a hard time. The unconditional love and encouragement provided by my family served as a secure anchor during the hard and easy times; I am blessed and thankful. I would also like to thank my brother **Ajin**, who took care of our parents in my absence.

Many thanks to my friends who have enriched my life and have allowed me to share my academic and personal experience. We have had lot of discussions and shared our concepts, ideas. We kept thinking about our research and future. Thanks to **Dr.Dinesh kumar** and **Naveen kumar** for the weekend get-together and cooking delicious foods.

I would like to thank the International coordinators **Dr. Jinna** and her support. She have organized many field trips for the foreigner which helped me to know better about Korea.

Last but not least, I would like to express my thanks to many amazing friends I have had and as well as to some friends I have lost along the way**: Dr. Kamal, Dr. Salim, Dr. Hari, Dr. Swapnil, Dr. Rajendran, Deva, Karthick, Robin,Superna and Cricket friends,** You all made me happy and this helped me feel like I am at home during my stay in Korea, Thank you all.

Dedication

This dissertation is dedicated to my Parents, for their love, support and encouragement throughout my life.